

FSFM: A Generalizable Face Security Foundation Model via Self-Supervised Facial Representation Learning

Gaojian Wang, Feng Lin*, Tong Wu, Zhenguang Liu, Zhongjie Ba, Kui Ren
 State Key Laboratory of Blockchain and Data Security, Zhejiang University
 Hangzhou High-Tech Zone (Binjiang) Institute of Blockchain and Data Security
 {wolo, flin, cocotwu, liuzhenguang, zhongjieba, kuiren}@zju.edu.cn
<https://fsfm-3c.github.io>

Abstract

*This work asks: with abundant, unlabeled real faces, how to learn a robust and transferable facial representation that boosts various face security tasks with respect to generalization performance? We make the first attempt and propose a self-supervised pretraining framework to learn fundamental representations of real face images, **FSFM**, that leverages the synergy between masked image modeling (MIM) and instance discrimination (ID). We explore various facial masking strategies for MIM and present a simple yet powerful CRFR-P masking, which explicitly forces the model to capture meaningful intra-region Consistency and challenging inter-region Coherency. Furthermore, we devise the ID network that naturally couples with MIM to establish underlying local-to-global Correspondence via tailored self-distillation. These three learning objectives, namely **3C**, empower encoding both local features and global semantics of real faces. After pretraining, a vanilla ViT serves as a universal vision Foundation Model for downstream Face Security tasks: cross-dataset deepfake detection, cross-domain face anti-spoofing, and unseen diffusion facial forgery detection. Extensive experiments on 10 public datasets demonstrate that our model transfers better than supervised pretraining, visual and facial self-supervised learning arts, and even outperforms task-specialized SOTA methods.*

1. Introduction

The human face plays a crucial role in daily life and computer vision. In parallel, the facial security landscape suffers from diverse digital and physical manipulations, notably face forgery and presentation attacks. Face forgery edits digital pixels while keeping realistic visual quality. With significant advances in generative models [34, 47, 60], the

abuse of this technology, aka deepfakes, could lead to severe trust crises. Presentation attacks use physical media, e.g., printed photos, image/video replays, or 3D masks, to spoof face recognition systems, risking real-life applications like face unlocking and payment. Thus, both academia and industry have been devoted to combating face forgery and presentation attacks with dedicated tasks: Deepfake Detection (DfD), Face Anti-Spoofing (FAS), and recently raised, Diffusion Facial Forgery detection (DiFF).

Current DfD and FAS methods aim to improve generalization to unseen datasets within their respective tasks. DfD methods mainly focus on digital forgery patterns, such as spatiotemporal inconsistency [3, 21, 108], region artifacts [48, 77, 113], and forgery augmentations [3, 77, 89, 113]. FAS methods [50, 62, 92, 133, 134] incorporate domain generalization (DG) techniques to discern physical spoof cues, e.g., paper textures and screen moire patterns. Given these incompatible digital and physical features, most studies treat DfD and FAS as separate face security tasks, i.e., **task-specific** and **hard to transfer**. Besides, until now, most DfD and FAS methods still follow fully supervised learning with diverse backbones [22, 28, 43, 95] that are initiated from scratch or supervised ImageNet (natural images) [25] pretraining. However, **fully supervised learning** requires large-scale annotated data or generative augmentations, which impose expensive resource costs and **limit scalability**. Moreover, initial weights that **lack facial representations** may **impede capability** and **generality** for face-related tasks [7, 130].

In contrast to supervised learning, self-supervised learning (SSL) takes pretext tasks for pretraining on unlabeled data, where masked image modeling (MIM) [5, 45, 114] and instance discrimination (ID, including contrastive learning [14, 16, 44] and distillation-based [11, 15, 36]) have proven superior performance in various vision tasks. As recent studies [81, 82, 135] suggest that MIM and ID are complementary, SOTA SSL methods [2, 17, 46, 55, 96, 128]

*Corresponding author

combine them to improve the visual representation of natural images. However, SSL progress for facial pretraining, especially security tasks, remains limited, raising **Q1: how can face security tasks benefit from self-supervised pretraining to learn scalable and generic representations?**

Although existing works introduce SSL to face security tasks, most focus on specific forgery or spoof patterns rather than transferable representations. In DfD, some methods [12, 13, 61, 89] synthesize forgeries from real faces to simulate forgery artifacts like blending, vulnerable to unknown forgery or spoof. Others [31, 41, 127] rely on audio-video datasets and multi-modal information, limiting their scalability. The latest work [123] combines MIM and ID to learn temporal consistency [136] from real face videos, but intra-frame representations fail for image-only forgery and replay videos with consistent temporal features. Conversely, FAS methods employ SSL to mine spoof cues using domain positives [73], domain-invariant semantics [129], or domain alignment [72], yet this FAS domain knowledge contributes less to detecting deepfake and diffusion forgery.

Recent advances in facial pretraining [7, 8, 32, 74, 130] demonstrate that task-agnostic facial representations transfer effectively to several face analysis tasks, such as expression and attribute recognition. However, these methods focus primarily on salient facial features that forgery and spoof faces also exhibit well, *i.e.*, overlook “realness” representations that go beyond normal facial analysis, thus hindering their extrapolation to face security tasks [130]. Furthermore, these methods commonly adopt intra-dataset evaluations for downstream tasks, whereas face security tasks call for cross-dataset generalization. These concerns raise **Q2: how to learn universal facial representations from real faces that transfer well to various face security tasks and improve downstream generalization?**

To bridge the above gap, instead of task-specific or unified [24, 121, 122] supervised learning, we propose learning the intrinsic properties of unlabeled real face images through SSL. Specifically, we introduce a simple yet effective CRFR-P facial masking strategy into a masked autoencoder [45] that directs attention to pixel-level contexts and region-level correlations, yielding a meaningful and challenging MIM task. By Covering a Random Facial Region (*e.g.*, eyes, nose) and Proportionally masking other regions, our CRFR-P promotes inter-region coherency and intra-region consistency in facial representations. For reliable face-level semantic alignment, we further integrate an ID network with MIM to establish local-to-global correspondence via elaborate self-distillation: the CRFR-P masked online view introduces spatial variance, the unmasked target view retains complete semantics, and Siamese representation decoders form a disentangled space. Thus, our framework, FSFM, leverages the synergy between MIM and ID to empower both local and global perception, learns a uni-

versal representation of real faces, transfers well to various face security tasks, and achieves superior generalization in cross-dataset DfD, cross-domain FAS, and unseen DiFF.

Our main contributions are:

- We propose a self-supervised pretraining framework to learn a fundamental representation of real faces, FSFM, which fully leverages the advantages of masked image modeling and instance discrimination for both local context perception and global semantic alignment.
- We design a simple yet powerful CRFR-P facial masking strategy for MIM to enhance meaningful intra-region Consistency and capture challenging inter-region Coherency, and we develop the ID network coupled with MIM to establish local-to-global Correspondence through elaborate self-distillation—namely, **3C**.
- We use a vanilla ViT as the encoder to learn transferable and robust facial representations; after pretraining, it serves as a universal vision foundation model for various downstream face security tasks, while previous methods adopt diverse backbones that vary from specific tasks.
- We conduct extensive experiments on prevalent face security tasks, including cross-dataset deepfake detection, cross-domain face anti-spoofing, and unseen diffusion facial forgery detection. Results on 10 public datasets show that our model generalizes better than supervised practices, visual and facial self-supervised pretraining arts, and notably, outperforms task-specialized SOTA methods. Moreover, FSFM benefits from pretraining with more abundantly unlabeled real faces (a free lunch).

2. Related work

Visual representation learning Masked image modeling (MIM) and instance discrimination (ID) are predominant pretext tasks for generative and discriminative self-supervised learning (SSL), respectively. MIM masks parts of an image and takes visible portions to restore the masked content, such as pixels [45, 114], visual tokens [5], or auxiliary features [109]. With a high masking ratio, the tokenizer-free MAE [45] achieves efficient pretraining. Follow-up studies [57, 63, 78, 88, 101] highlight masking strategies and region-based learning. ID employs Siamese networks to pull positive pairs closer, mainly including contrastive learning (CL) and distillation (DIS) paradigms to avoid collapse. CL [14, 16, 44] simultaneously pushes negative pairs away. DIS [11, 15, 36] is negative-free and adopts asymmetric architecture to align representations between two branches. As recent studies [81, 82, 135] suggest that MIM and ID complement each other, cutting-edge SSL methods increasingly combine MIM with ID via Siamese designs [1, 2, 30, 96], including CL [46, 55, 64, 119] and DIS [4, 17, 128, 131], for natural vision representations.

Facial representation learning Several works [66, 79, 93, 97, 100] explore facial SSL to reduce overfitting and im-

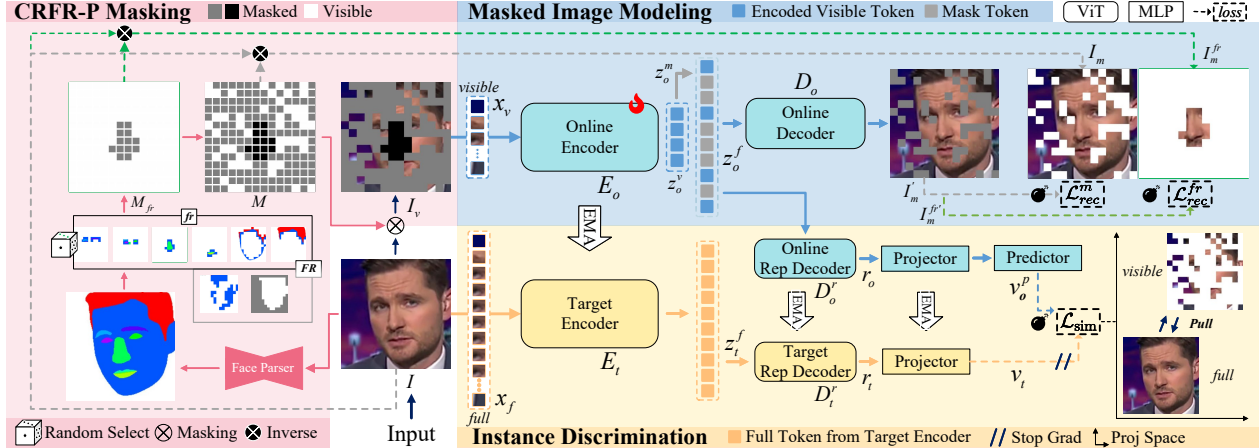


Figure 1. **Overview of FSFM** self-supervised pretraining framework for learning foundational representations of real faces ($3C$). Guided by the **CRFR-P masking** strategy, the **masked image modeling (MIM)** network captures *intra-region Consistency* with \mathcal{L}_{rec}^m and enforces *inter-region Coherency* via \mathcal{L}_{rec}^{fr} , while the **instance discrimination (ID)** network collaborates to promote *local-to-global Correspondence* through \mathcal{L}_{sim} . After pretraining, the online encoder E_o (a vanilla ViT) is applied to boost downstream face security tasks.

prove performance, but they remain tailored for a single task, i.e., task-specific. VLP-based FaRL [130] leverages web image-text CL with MIM to transfer across various facial tasks, but it requires image-text pairs and additional computation overhead, and the text captions tend to describe context rather than face details. Recent SSL efforts aim to learn general facial representations by MIM [8, 103], CL [7, 74, 103], DIS [32, 103] for various downstream tasks, such as expression [7, 8, 32, 74], attribute [8, 32], and AU [7, 74] recognition, alignment [7, 32, 103], etc. Despite excelling in normal face analysis, these methods lack generality for face security tasks as they ignore facial ‘realness’ representations.

3. FSFM framework

We now describe the proposed FSFM pretraining framework in Fig. 1, which aims to learn intrinsic and transferable representations of real faces. The pretext tasks for self-supervised learning (SSL) include masked image modeling (MIM) and instance discrimination (ID). Driven by our CRFR-P masking strategy (Sec. 3.1), the MIM network ($E_o \circ D_o$), a naive masked autoencoder (MAE) [45], reconstructs the masked face to capture intra-region consistency and enforce inter-region coherency (Sec. 3.2). Meanwhile, the ID network employs the MIM encoder in the online branch ($E_o \circ D_o^r \circ proj \circ pred$) and establishes local-to-global correspondence, where the target branch ($E_t \circ D_t^r \circ proj$) guides global semantics (Sec. 3.3). These three objectives, termed $3C$, endow the online encoder with pixel-level context perceptiveness, region-level relation awareness, and instance-level face invariance.

3.1. CRFR-P masking

The mask sampling strategy plays a key role in MIM for both representation quality and downstream performance, and also provides the local view for our ID network.

Motivation Random masking with a high mask ratio is widely used in natural [45, 114] and facial [103, 130] MIM, but it lacks domain-specific knowledge, limiting pretrained facial models. Given that human faces, our sole focus, comprise well-defined parts with distinct textures, we turn to explicitly segment the facial semantics for reasonable and efficient mask sampling rather than additional learning modules [57, 63, 88, 101]. Similarly, MARLIN [8] uses an off-the-shelf face parser to divide facial parts and introduces the Fasking mask for face video MIM. We adapt Fasking to images as Fasking-I in Fig. 2 (b): it divides facial parts into $\{left\text{-}eye, right\text{-}eye, nose, mouth, hair, skin, background\}$, prioritizing masking non-skin and non-background regions. However, Fasking-I struggles to capture sufficient details solely from background and skin patches, rendering it unsuitable for face security tasks. Motivated by FACS [29] and psychological studies [42, 85], we explore more effective masking strategies to learn local facial representations.

Intuition of intra-region consistency and inter-region coherency. As shown in Fig. 2, random masking and Fasking-I are prone to fully mask small but informative regions (e.g., eyes), hindering accurate learning of textures therein (e.g., pupils, iris). For intra-region consistency, we introduce FRP (Facial Region Proportional) masking that randomly masks an equal portion of patches in each region. FRP ensures all regions have visible patches, thus enabling attention to the same region when restoring masked patches. However, a potential shortcut, restoring a region’s masked patches directly from its unmasked patches, may lead to a trivial re-

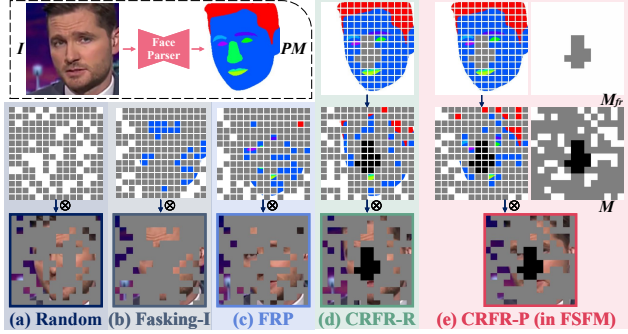


Figure 2. Comparison of masking strategies for face images (75% masking ratio). (a) Random masking. (b) Fasking-I, adapted from [8], priority masking regions $\notin \{\text{bg, skin}\}$. (c) Our FRP: Proportional masking within each Facial Region $\in \{FR\}$. (d) Our CRFR-R: Covering a Random Facial Region $\in \{fr\}$ and then Random masking other patches. (e) Our CRFR-P: Covering a Random Facial Region $\in \{FR\}$ and then Proportional masking other highlights fr . All masks are binary (black solely highlights fr).

construction task and ignore cross-region correlations. In this regard, we formulate CRFR-R (Covering a Random Facial Region followed by Random) masking for inter-region coherency. As the fully masked region can only be derived from visible patches outside it, CRFR-R encourages learning its relationship w.r.t. other regions. Yet, the subsequent random masking may still obscure other small informative regions, undermining the desired consistency within them. FRP and CRFR-R, our preliminary masking strategies, have individual limitations but complement each other.

CRFR-P Masking Based on the above insights, we propose CRFR-P (Covering a Random Facial Region followed by Proportional) masking strategy, shown in Fig. 1 and Alg. 1. CRFR-P first divides facial parts into predefined regions FR using an off-the-shelf face parser. Next, it masks all patches within a randomly selected region $fr \notin \{\text{skin, background}\}$ and obtains the facial region mask M_{fr} . Then, based on the number of masked patches and the overall masking ratio r , it randomly masks an equal portion of patches across the remaining $\{FR - fr\}$ regions to generate the image mask M . Finally, it returns both M and M_{fr} . CRFR-P naturally resolves the core challenge: simultaneously promoting intra-region consistency and inter-region coherency.

Strength Despite its simple design, CRFR-P masking poses a nontrivial and meaningful facial MIM task by effectively directing attention to critical facial regions with appropriate range and diversity. It not only avoids the trivial solution (shortcut) but also captures the intrinsic properties of real faces. In the supplementary material, we reveal key attention differences when applying different facial masking strategies to naive MAE pretraining.

Algorithm 1 CRFR-P Masking Strategy

Input: Real face image I , Masking ratio r
Output: Image mask M , Facial region mask M_{fr}

- 1: $PM \leftarrow \text{Face_Parser}(I)$
- 2: $P_{pm} \in \mathbb{R}^N \leftarrow \text{patchify}(PM)$
- 3: $M, M_{fr} \leftarrow [0] \in \mathbb{R}^N, [0] \in \mathbb{R}^N$
- 4: $FR \leftarrow \{\text{eyebrows} \supseteq [\text{right eyebrow, left eyebrow}], \text{eyes} \supseteq [\text{right eye, left eye}], \text{mouth} \supseteq [\text{upper lip, inner mouth, lower lip}], \text{face boundary} \supseteq [\text{skin} \cap \text{background}, \text{skin} \cap \text{hair}], \text{nose, hair, skin, background}\}$
- 5: Randomly select a $fr \in \{FR - \{\text{skin, background}\}\}$
- 6: $M_{fr}[P_{pm} \cap fr] \leftarrow 1$ \triangleright Covering a Random Facial Region
- 7: **if** $\sum M_{fr} > N \cdot r$ **then** \triangleright Extreme-case
- 8: Randomly unmask $(\sum M_{fr} - N \cdot r)$ patches in M_{fr}
- 9: $M \leftarrow M_{fr}$
- 10: **break**
- 11: **end if**
- 12: $M \leftarrow M_{fr}$
- 13: **for** $pr \in \{FR - \{fr\}\}$ **do** \triangleright Proportional masking in other regions
- 14: $r = (N \cdot r - \sum M) / (N - \sum M)$
- 15: $M[(P_{pm} \cap pr) \cdot r] \leftarrow 1$
- 16: **end for**
- 17: **Return:** M, M_{fr}

3.2. MIM for facial region perception

In a nutshell, the MIM network ($E_o \circ D_o$) in FSFM is an MAE [45] model guided by our CRFR-P masking strategy. Below, let $x_f = \{x_i\}_{i=1}^N$ denote the full set of N non-overlapping patches split from the input face image I .

Online Encoder E_o only operates on the visible patches $x_v \leftarrow M \odot x_f$ and maps x_v into latent features z_o^v , where \odot means the element-wise product for masking and \leftarrow selects the visible ones. The online encoder first embeds x_v by a linear projection as patch embeddings, and adds corresponding positional embeddings p_v . It then processes the fused embeddings through a series of transformer blocks to obtain: $z_o^v = E_o(x_v + p_v)$.

Online Decoder D_o reconstructs the input image pixels. It first combines encoded visible tokens z_o^v with mask tokens z_o^m , and adds relative positional embeddings to form the full tokens set z_o^f . The online decoder consists of another sequence of transformer blocks that receives z_o^f as input, followed by a linear layer to restore the masked patches: $z_o^v = E_o(x_v + p_v)$.

MIM Objective Following [45], we take normalized pixels as the reconstruction target and minimize the mean squared error (MSE) loss on masked patches between the prediction I'_m and the original one $I_m \leftarrow (1 - M) \odot I$:

$$\mathcal{L}_{rec}^m = \frac{1}{N_m} \sum_{i=1}^{N_m} \left(I_m^{(i)} - I'_m{}^{(i)} \right)^2, \quad (1)$$

where $N_m = N \times r = \sum M$ is the number of masked patches. Our CRFR-P masking provides an additional mask M_{fr} , covering all patches in a randomly selected facial region $I_m^{fr} \leftarrow (1 - M_{fr}) \odot I$. To enhance inter-region coherency and prevent trivial solutions, we add another reconstruction

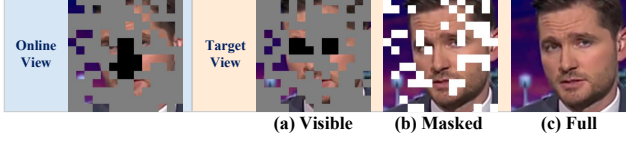


Figure 3. Comparison of different target views. (a) Visible patches from a different mask. (b) Masked patches from the same mask. (c) Full patches without masking.

loss only on the masked patches of the facial region fr :

$$\mathcal{L}_{rec}^{fr} = \frac{1}{N_{fr}} \sum_{j=1}^{N_{fr}} \left(I_m^{fr(j)} - I_m^{fr'(j)} \right)^2, \quad (2)$$

where $N_{fr} = \sum M_{fr}$ is the number of patches in fr , and $I_m^{fr'} \leftarrow (1 - M_{fr}) \odot I_m'$. The overall MIM objective updates the MAE network ($E_o \circ D_o$) as a weighted sum:

$$\mathcal{L}_{rec} = \mathcal{L}_{rec}^m + \lambda_{fr} \mathcal{L}_{rec}^{fr}. \quad (3)$$

3.3. ID for local-to-global self-distillation

In a nutshell, the ID network in FSFM employs symmetric designs between the online and target branches w.r.t. the encoder and representation decoder, as well as asymmetric designs w.r.t. the input view, projection head, negative-free loss, and model update rate. These designs focus on more precise and reliable semantic alignment for face security tasks, distinguishing our method from previous works that also integrate ID into MIM or degraded image input.

Target Encoder E_t takes full patches $x_f = \{x_i\}_{i=1}^N$ as the target view to produce target latent features z_t^f that guide the online encoder E_o in learning holistic representations. Among the target view options in Fig. 3, using full patches enables complete facial semantic embedding for local-to-global representation learning. Thus, the target encoder E_t serves as a teacher that shares the same structure as the student E_o . Similarly, with positional embeddings p_f of full patches, E_t yields global embeddings: $z_t^f = E_t(x_f + p_f)$.

Online and Target Rep Decoder The online rep decoder D_o^r maps the full tokens z_o^f to online representations r_o . Unlike the online decoder D_o , which restores pixel values, D_o^r reconstructs the masked token representations to align with the uncorrupted target, using significantly shallower transformer blocks followed by a linear layer that predicts features. The token features are output by a mean pooling as the online representations: $r_o = D_o^r(z_o^f)$. In the target branch, the momentum encoder E_t is updated by past iterations of the online encoder E_o , which also serves MIM. If r_o is directly matched with target embeddings z_t^f , the model may struggle to fit high-level target features while restoring low-level pixels. Thus, a target rep decoder D_t^r with the same structure as D_o^r is added to represent the target features in the same disentangled space: $r_t = D_t^r(z_t^f)$.

ID Objective Following [15, 16, 36], we use a projector and a predictor to transform r_o into a lower-dimensional vector

v_o^p , and apply only a projector to r_t to obtain v_t . We then minimize the negative cosine similarity [15] between the ℓ_2 -normalized v_o^p and v_t :

$$\mathcal{L}_{sim}(v_o^p, \text{sg}[v_t]) = -\frac{v_o^p}{\|v_o^p\|_2} \cdot \frac{v_t}{\|v_t\|_2}, \quad (4)$$

where $\text{sg}[\cdot]$ is a stop-gradient, *i.e.*, gradients are only calculated w.r.t. the online branch ($E_o \circ D_o^r \circ \text{proj} \circ \text{pred}$). The parameters θ_t of the target branch ($E_t \circ D_t^r \circ \text{proj}$) are updated via an exponential moving average (EMA) [36]: $\theta_t \leftarrow \tau \theta_t + (1 - \tau) \theta_o$. Note that \mathcal{L}_{sim} is asymmetric due to the different input views of the online and target branches, unlike the symmetrized designs [11, 15, 16, 36].

3.4. Overall pretraining objective

Overall Loss FSFM learns foundational representations of real faces from both the MIM (Eq. (3)) and ID (Eq. (4)) pretext tasks. Thus, the overall pretraining objective is a combined loss weighted by λ_{cl} :

$$\mathcal{L} = \mathcal{L}_{rec} + \lambda_{cl} \mathcal{L}_{sim} \stackrel{\text{Eq. (3)}}{=} \mathcal{L}_{rec}^m + \lambda_{fr} \mathcal{L}_{rec}^{fr} + \lambda_{cl} \mathcal{L}_{sim}. \quad (5)$$

4. Experiments

In downstream face security tasks, including deepfake detection (DfD, Sec. 4.2), face anti-spoofing (FAS, Sec. 4.3), and diffusion facial forgery detection (DiFF, Sec. 4.4), we demonstrate the effectiveness of FSFM by asking: **Q1**: Does our facial representation generalize better than common weight initialization practices? **Q2**: Is our method superior to other SSL methods for natural vision or normal facial analysis? **Q3**: Can our pretrained model outperform SOTA specialized methods with only simple fine-tuning? We further ablate FSFM (Sec. 4.5) and present visualizations (Sec. 4.6) to ascertain our contributions. We include more pretraining, finetuning details, ablations, and visualizations in the supplementary material.

4.1. Pretraining setups and baselines

Pretraining Data and Preprocessing We use the VG-Face2 [10] dataset (VF2, $\sim 3.3\text{M}$ images) for pretraining. We utilize the DLIB [59] for face detection and cropping with a 30% addition margin, and the FACER [130] toolkit for face parsing instead of alignment. Cropped face images are resized to 224×224 , and parsing maps are saved as binary stream files for efficient CRFR-P masking.

Model Architecture Our MIM network is a vanilla MAE [45] with ViT-B/16 as the default encoder E_o . In the ID network: rep decoders, D_o^r and D_t^r are 2-layer ViT blocks with the same width as the encoder; the projector and predictor are 2-layer MLPs following BYOL [36]. After pretraining, we only use E_o as the backbone and add a task-specific head for downstream finetuning.

Implementation We set the mask ratio r to 0.75. We use no data augmentation (not even crop or flip used in [45])

Method	Pretrain or Init	Train Set	Test Set Video-level AUC(%) [†]				Avg. Δ Ours	Method	Pretrain or Init	Train Set	Test Set Frame-level AUC(%) [†]				Avg. Δ Ours
			CDFV2	DFDC	DFDCP	WDF					CDFV2	DFDC	DFDCP	WDF	
Base model							Base model								
Xception [22]	Sup(IN)	FF++	76.39	70.62	72.24	76.11	14.0 [†]	Xception [22]	Sup(IN)	FF++	69.52	68.20	68.94	68.83	15.1 [†]
EfficientNet-B4 [95]	Sup(IN)	FF++	79.81	71.85	66.95	76.42	14.1 [†]	EfficientNet-B4 [95]	Sup(IN)	FF++	73.37	69.47	64.37	71.95	14.2 [†]
ViT-B [28]	Scratch	FF++	64.08	66.73	72.62	60.36	21.9 [†]	ViT-B [28]	Scratch	FF++	61.14	64.27	69.00	60.68	20.2 [†]
ViT-B [28]	Sup(IN)	FF++	86.24	74.48	82.11	81.20	6.9 [†]	ViT-B [28]	Sup(IN)	FF++	77.43	71.09	74.07	75.86	9.4 [†]
MAE [45] ViT-B	SSL(IN)	FF++	79.51	75.93	87.10	80.96	7.0 [†]	MAE [45] ViT-B	SSL(IN)	FF++	72.64	72.18	79.81	73.94	9.4 [†]
DINO [11] ViT-B	SSL(IN)	FF++	80.47	76.90	84.64	82.06	6.9 [†]	DINO [11] ViT-B	SSL(IN)	FF++	73.88	72.78	77.31	75.08	9.2 [†]
MCF [103] ViT-B	SSL(LFc)	FF++	80.25	73.61	82.55	79.79	8.8 [†]	MCF [103] ViT-B	SSL(LFc)	FF++	73.16	69.63	75.78	74.10	10.8 [†]
FSFM ViT-B (Ours)	SSL(VF2)	FF++	91.44	83.47	89.71	86.96	-	FSFM ViT-B (Ours)	SSL(VF2)	FF++	85.05	80.20	85.50	85.26	-
SOTA specialized method (Venue)							SOTA specialized method (Venue)								
SBIs [89] (CVPR'22) [‡]	Init(IN)	SD	93.18	72.42	86.15		4.3 [†]	OST [13] (NIPS'22) [‡]	Init(IN)	FF++	74.80		83.30		6.2 [†]
RealForensics [41] (CVPR'22)	SSL(LRW)	FF++	86.90	75.90			6.1 [†]	FInfer [51] (AAAI'22) [‡]	Init(IN)	FF++	70.60		70.39	69.46	15.1 [†]
HCLC [38] (ECCV'22)	Init(IN)	FF++	79.00		69.21		16.5 [†]	PEL [37] (AAAI'22) [‡]	Init(IN)	FF++	69.18	63.31		67.39	16.9 [†]
SeeABLE [61] (ICCV'23) [‡]	SSL(SD)	SD	87.30	75.90	86.30		5.0 [†]	SLADD [12] (CVPR'22) [‡]	Init(IN)	SD	79.70		81.80		4.5 [†]
TALL [116] (ICCV'23)*	Init(IN)	SD	90.79	76.78			3.7 [†]	RECCE [9] (CVPR'22) [‡]	Init(IN)	FF++	68.71	69.06		64.31	16.1 [†]
AUNet [3] (CVPR'23) [‡]	Init(IN)	SD	92.77	73.82	86.16		4.0 [†]	UIA-ViT [136] (ECCV'22)*	SSL(FF)	FF++	82.41		75.80		6.2 [†]
SLF [21] (CVPR'24)	FTCN	FF++	89.00				2.4 [†]	UAL [112] (MM'23)*	Init(IN)	FF++	82.84			70.13	8.7 [†]
MLR [48] (CVPR'24)*		FF++	91.56	75.17		73.41	7.2 [†]	NoiseDF [102] (AAAI'23)	RIDNet	FF++	75.89		63.89		15.3 [†]
LAA-Net/BI [77] (CVPR'24) [‡]	Init(IN)	SD	86.28		69.69	57.13	18.3 [†]	GS [40] (ICCV'23) [‡]	FF++	84.97		81.65		1.8 [†]	
LAA-Net/SBI [77] (CVPR'24) [‡]	Init(IN)	SD	95.40		86.94	80.03	1.9 [†]	UCF [117] (ICCV'23) [‡]	Init(IN)	FF++	82.40		80.50		3.7 [†]
LSDA [118] (CVPR'24) [‡]	Init(IN)	FF++	91.10	77.00			3.4 [†]	SFDG [104] (CVPR'23) [‡]	Init(IN)	FF++	75.83	73.64		69.27	10.6 [†]
FPG [113] (MM'24) [‡]	Init(IN)	SD	94.49	74.75	87.24		2.7 [†]	IID [53] (CVPR'23)	CF(WF)	FF++	83.80		81.23		2.8 [†]
NACO [123] (ECCV'24)*	SSL(VC2)	FF++	89.50	76.70			4.4 [†]	LSDA [118] (CVPR'24) [‡]	Init(IN)	FF++	83.00	73.60	81.50		4.2 [†]

Abbreviation: Sup-Supervised SSL-Self-Supervised Init-weight initialization Dataset: IN-ImageNet LRW-LipReading in the Wild/facial VC2-VoxCeleb2/facial CF(WF)-CosFace(WebFace)/facial Backbone(or modified): † Xception ‡ EfficientNet-B4 * ViT or transformer-based

Table 1. Cross-dataset evaluation on deepfake detection (DfD). Left: video-level, Right: frame-level. All base models are trained on FF++ (c23) and tested on unseen datasets. For a fair comparison, the results of SOTA specialized methods are cited from their original papers. Avg. Δ Ours denotes the average AUC difference between our FSFM and other methods on their test sets. **Best results**, second-best.

during pretraining. We empirically set the loss weights λ_{fr} , λ_{cl} to 0.007, 0.1, respectively. The EMA momentum coefficient follows [36]. We pretrain our model from scratch for 400 epochs. Other setups follow MAE [45] defaults.

Pretrained Base Models To answer Q1 and Q2, we include the following pretrained models based on availability (official weights), fairness (vision-only ViT-B/16 backbone), and relevance: 1) ViT-B Scratch [28], to discern pretraining effects versus the backbone itself; 2) ViT-B Sup(IN) [28], supervised ImageNet pretraining, the most common weight initialization for face security tasks; 3) MAE SSL(IN) [45], our MIM network, the baseline across all experiments, including ablations; 4) DINO SSL(IN) [11], a self-distillation method for ID, which also encourages local-to-global correspondence; 5) MCF SSL(LFc) [103], a SOTA facial representation model for face analysis tasks, which also combines MIM and ID and is pretrained on the large-scale LAION-FACE-cropped dataset ($\sim 20M$ images). For downstream tasks, we compare our FSFM with these models by initializing the backbone with their pretrained weights and keeping other settings identical. We employ end-to-end fine-tuning for all models, facilitating a fair comparison with SOTA specialized methods to answer Q3.

4.2. Deepfake detection

Setting To evaluate the generalizability of our method across diverse DfD scenarios, we follow the challenging cross-dataset setup. Specifically, we train *one detector* on the FaceForensics++ (FF++, c23/HQ version) [84] dataset and test it on unseen datasets: CelebDF-v2 (CDFv2) [65], Deepfake Detection Challenge (DFDC) [27], Deepfake Detection Challenge preview (DFDCp) [26], and Wild Deepfake (WDF) [137]. For a fair comparison, we report the

Area Under Curve (AUC) at both frame-level and video-level, the most widely used metric for DfD, in Tab. 1.

Comparison with Base Models As shown in Tab. 1, our FSFM significantly outperforms all base models on unseen deepfakes at both frame and video levels: 1) It surpasses Sup(IN) baselines, including ViT-B, Xception, and EfficientNet-B4, which are common practices for DfD. This suggests that our pretrained model provides a strong initialization for the detector. 2) MIM-based MAE and ID-based DINO show comparable performance but vary across different datasets, mainly because MIM focuses on local patterns while ID operates globally [135]. FSFM outperforms both MAE and DINO, indicating the effectiveness of learning both local and global facial representations. 3) Notably, FSFM, pretrained on 3M VF2, consistently surpasses MCF, which is pretrained on 20M facial images and also incorporates MIM and ID. Although MCF achieves SOTA performance in face analysis tasks, its generalization to DfD is even worse than ViT, MAE, and DINO pretrained on natural images. 4) These comparisons demonstrate that FSFM effectively learns fundamental real face representations that are sensitive to deepfakes and generalizable for detection.

Comparison with SOTA Specialized Methods As shown by Avg. Δ Ours in Tab. 1, FSFM consistently outperforms all counterparts, achieving the best overall performance. Our model surpasses both transformer-based and SSL-based competitors that are task-specific. In particular, our method outperforms SSL-based NACO, a most recent work [123] that also learns consistent representations of real face videos, and it further combines ViT-B with CNN. Our model also performs best across unseen datasets except in video-level testing on CDFV2, where some models trained on synthetic data show slightly better results. These

Method	Pretrain or Init	DG FAS Technique					OCI→M		OMI→C		OCM→I		ICM→O		Avg.	
		DM	AL	CL	ML	PL	HTER↓	AUC↑	HTER↓	AUC↑	HTER↓	AUC↑	HTER↓	AUC↑	HTER↓	AUC↑
Base model																
ViT-B [28]	Scratch						15.37	90.73	35.37	68.23	14.75	94.18	31.65	71.55	24.28	81.17
ViT-B [28]@ECCV'22 [54]	Sup(IN)						3.52	98.74	2.42	99.52	8.45	96.91	11.86	94.62	6.56	<u>97.44</u>
MAE [45] ViT-B	SSL(LN)						10.32	94.87	15.91	89.96	15.54	91.13	16.51	90.29	14.57	91.56
DINO [11] ViT-B	SSL(LN)						6.73	97.15	13.44	93.90	14.27	93.56	15.55	90.99	12.50	93.90
MCF [103] ViT-B	SSL(LFc)						4.00	<u>98.84</u>	8.46	96.90	8.02	97.39	10.70	95.64	7.80	97.19
FSFM ViT-B (Ours)	SSL(VF2)						3.78	99.15	3.16	<u>99.41</u>	4.63	99.03	7.68	97.11	4.81	98.68
SOTA specialized method (Venue)																
MADDG [87] (CVPR'19)†	Scratch	✓	✓	✓			17.69	88.06	24.50	84.51	22.19	84.99	27.98	80.02	23.09	84.40
SSDG-R [56] (CVPR'20)‡	Init(IN)		✓	✓			7.38	97.17	10.44	95.94	11.71	96.59	15.61	91.54	11.29	95.31
AMEL [132] (MM'22)†	Scratch	✓			✓		10.23	96.62	11.88	94.39	18.60	88.79	11.31	93.96	13.01	93.44
FGHV [70] (AAAI'22)‡	Depth Net		✓	✓			9.17	96.92	12.47	93.47	16.29	90.11	13.58	93.55	12.88	93.51
PatchNet [99] (CVPR'22)‡	Init(IN)		✓	✓			7.10	98.46	11.33	94.58	13.40	95.67	11.82	95.07	10.91	95.95
SSAN-R [107] (CVPR'22)‡	Init(IN)	✓	✓	✓			6.67	98.75	10.00	96.67	8.88	96.79	13.72	93.63	9.82	96.46
UDG-FAS [73] (ICCV'23)‡	SSL(LOO)		✓	✓			7.14	97.31	11.44	95.59	6.28	98.61	12.18	94.36	9.26	96.47
UDG-FAS [73] (ICCV'23)‡	Init(IN)		✓	✓			5.95	98.47	9.82	96.76	5.86	98.62	10.97	95.36	8.15	97.30
IADG [133] (CVPR'23)†	Scratch	✓	✓	✓			5.41	98.19	8.70	96.44	10.62	94.50	8.86	<u>97.14</u>	8.40	96.57
SAFAS [92] (CVPR'23)‡	Init(IN)		✓	✓			5.95	96.55	8.78	95.37	6.58	97.54	10.00	96.23	7.83	96.42
GAC-FAS [62] (CVPR'24)‡	Init(IN)		✓	✓			5.00	97.56	8.20	95.16	4.29	<u>98.87</u>	<u>8.60</u>	97.16	<u>6.52</u>	97.19
HPDR [50] (CVPR'24)‡	Depth Net				✓		4.58	96.02	11.30	94.42	11.26	92.49	9.93	95.26	9.27	94.55
TTDG [134] (CVPR'24)†	Scratch	✓	✓				7.91	96.83	8.14	96.49	6.50	97.98	10.00	95.70	8.14	96.75

Abbreviation: Sup-Supervised SSL-Self-Supervised Init-weight initialization IN-ImageNet DG-Domain Generalization

DG FAS Technique: DM-Depth Maps AL-Adversarial Learning CL-Contrastive Learning (or triplet, similarity loss) ML-Meta Learning PL-Prototype Learning

Backbone(or modified): † CNN-based network defined in MADDG ‡ Dense Net # ResNet-18

Table 2. Cross-domain evaluation on face anti-spoofing (FAS). For a fair comparison, the results of SOTA specialized methods are cited from their original papers. **Best results, second-best.**

Method	Pretrain or Init	Test Subset (AUC%↑)					Avg. w/o FF++
		FF++	T2I	I2I	FS	FE	
ViT-B [28]	Scratch	92.02	62.19	69.99	60.87	67.30	65.09
ViT-B [28]	Sup(IN)	99.15	33.38	35.83	52.20	55.42	44.21
MAE [45] ViT-B	SSL(IN)	99.25	33.01	32.88	47.77	58.70	43.09
DINO [11] ViT-B	SSL(IN)	99.30	33.85	36.02	60.37	63.18	48.35
MCF [103] ViT-B	SSL(LFc)	99.39	39.09	38.67	34.35	56.02	42.03
FSFM ViT-B	SSL(FF++_o)	99.31	61.74	71.91	71.31	78.98	70.99

Table 3. Cross-dataset evaluation on the DiFF benchmark [19]. All models are trained only on the FF++_DeepFake (c23) subset [84].

methods (AUNet, FPG, and LAA-Net with SBIs) simulate pseudo-fake features, especially blending artifacts similar to face-swapping in CDFV2, but struggle with forgeries lacking such clues. Moreover, our method yields notable gains on more challenging DFDC and WDF datasets, which contain diverse unknown real-world manipulations. Remarkably, our FSFM, a vanilla ViT-B base model, achieves SOTA performance without any specialized network modules or tailored data generation for deepfake detection.

4.3. Face anti-spoofing

Setting To evaluate the transferability of our method for FAS under significant domain shifts, we use four widely used benchmark datasets: MSU-MFSD (M) [110], CASIA-FASD (C) [126], Idiap Replay-Attack (I) [20], and OULU-NPU (O) [6]. We treat each dataset as the target domain and apply the leave-one-out (LOO) cross-domain evaluation. As prior work [54] also finetunes vanilla ViT-B for this protocol, we follow its 0-shot setting by initializing weights from our FSFM and base models. We report mean HTER (Half Total Error Rate) and AUC over 5 runs in Tab. 2.

Comparison with Base Models Our FSFM achieves the best average performance among base models, with several key observations: 1) Simple finetuning on ViT-B Sup(IN) enhances FAS generalization, as noted in [54, 134]. 2) Gen-

eral SSL methods, including MIM-based MAE [45] and ID-based DINO [11], perform worse than ViT-B Sup(IN), with MAE showing notable declines, echoing the claims in [120]. 3) With large-scale facial data for SSL, MCF outperforms MAE and DINO for FAS. However, similar to DfD, it still falls short of the ViT-B Sup(IN) baseline in average metrics, once again underscoring the gap between normal face analysis and security tasks. 4) Overall, our FSFM improves the generalizability of ViT for cross-domain FAS, effectively modeling credible features of live (real) faces.

Comparison with SOTA Specialized Methods Our FSFM ViT-B exhibits superior performance over domain generalization (DG) FAS methods using various CNNs. Notably, this comparison adheres to the baseline [54]: although supplementary data (CelebA-Spoof [124]) is included for finetuning ViT-B, no auxiliary supervision or DG techniques, e.g., depth map (DM) or adversarial learning (AL), are employed—only a standard cross-entropy loss. Additionally, we follow other ViT-based FAS methods [67, 106, 134] without including CelebA-Spoof, with comparisons provided in the supplementary material.

4.4. Diffusion facial forgery detection

Setting To further investigate the adaptability of our method against emerging unknown facial forgeries, we adopt cross-distribution testing using the recently released DiFF [19] benchmark. This dataset contains high-quality face images synthesized by 13 SOTA diffusion models across four subsets: T2I (Text-to-Image), I2I (Image-to-Image), FS (Face Swapping), and FE (Face Editing). We train only on the FF++_DeepFake (c23) subset and report AUC results on the DiFF testing subsets. This evaluation is more challenging than typical DfD (Sec. 4.2), as both the unseen manipula-

Component	C^1	C^2	C^3	Deepfake Detection		Face Anti-spoofing	
				F-AUC \uparrow	V-AUC \uparrow	HTER \downarrow	AUC \uparrow
MAE & Masking Strategy (w/o ID Network)							
&Random (base)				74.19	79.51	19.05	87.42
&Fasking-I [8]				73.80	78.33	17.81	87.75
&FRP	✓			75.43	81.21	17.96	87.61
&CRFR-R		✓		75.01	80.70	18.28	87.34
&CRFR-P	✓	✓		76.11	81.58	17.85	88.11
ID & Target View (w/ MAE&CRFR-P)							
&Visible	✓	✓		75.54	81.50	18.22	87.95
&Masked	✓	✓		76.35	81.86	18.41	87.77
&Full (FSFM)	✓	✓	✓	76.39	82.31	17.44	88.26
Design				Setting			
Online&Target			0 & 0	75.63	81.48	18.37	86.77
Rep Decoder			2 & 0	75.74	81.14	18.54	87.22
(D_o^f & D_t^f)			1 & 1	75.06	80.68	18.86	87.64
Blocks			2 & 2	76.39	82.31	17.44	88.26
			3 & 3	75.08	80.71	17.93	87.80
Online&Target			crop+flip&none	75.93	81.54	18.24	87.04
Data (I_o&I_t)			none&crop+flip	73.39	78.80	19.13	86.11
Augmentation			none&none	76.39	82.31	17.44	88.26
			InfoNCE	75.10	80.60	18.24	87.37
Loss for ID			MSE ([36]-like)	74.19	79.34	18.09	88.21
			Asym. Eq. (4)	76.39	82.31	17.44	88.26
pretraining data				Size			
Data size			FF++ $_{\text{.o}}$ (0.1M)	76.39	82.31	17.44	88.26
(images)			YTF(0.6M) [111]	79.51	83.86	16.23	93.13
			VF2 (3.3M)	84.00	87.89	4.81	98.68

Table 4. Ablations on deepfake detection (DfD) and face anti-spoofing (FAS) with average metrics. If not specified, the model is pretrained on FF++ $_{\text{.o}}$. Default settings are shaded in gray.

tions and generative models are significantly different.

Comparison In Tab. 3, our model significantly outperforms other ViT detectors. Pretrained base models perform even worse than the model trained from scratch. This arises from severe overfitting to the deepfake distribution, which hinders discerning diffusion-generated faces. In contrast, our model benefits from fundamental representations of real faces that are not specific to forgery types. The substantial improvement in this new task highlights the robustness of our method in out-of-distribution scenarios.

4.5. Ablation studies

We conduct extensive ablations to evaluate the effectiveness of each component. In this subsection, unless otherwise stated, we pretrain the ViT-B/16 network on the FF++ $_{\text{.o}}$ dataset, which includes ~ 0.11 M real face images extracted from 720 training and 140 validation videos in the FF++ (c23) Youtube subset [84]. We present the average generalization performance on DfD and FAS in Tab. 4.

Effect of 3C We first evaluate facial masking strategies in the vanilla MAE. Both our preliminary FRP and CRFR-R outperform random masking, validating the significance of intra-region consistency (C^1) and inter-region coherency (C^2), respectively. Further, our CRFR-P emerges as the most effective, showing that both C^1 and C^2 are critical and complementary for robust facial representation. Building on MAE&CRFR-P, we incorporate the ID network with varied target views (Fig. 3). The improved performance with &Full confirms the benefit of local-to-global correspondence (C^3) guided by complete facial semantics.

Effect of Key Designs 1) Blocks of D_o^f & D_t^f A lightweight

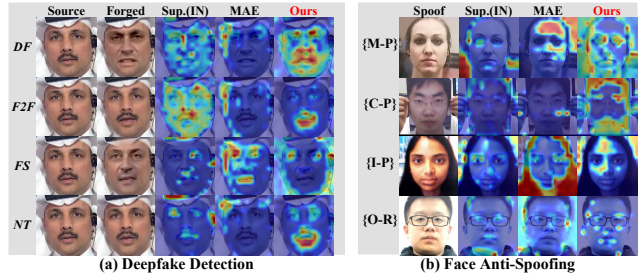


Figure 4. CAM Visualization. (a) DfD on various manipulations from FF++ [84]. (b) FAS on the MCIO protocol. FSFM highlights forgery artifacts and spoofing clues. Images are from the test set.

2-layer Rep decoder in both the online and target branches (2&2) achieves a better balance between complexity and generalization, outperforming 1&1 and 3&3. Omitting the Rep decoder (0&0) or adding it only to the target branch (2&0) degrades performance, supporting the importance of bridging feature distribution in a disentangled space. **2) Data Augmentation** FSFM performs best without data augmentation (none&none). Unlike many SSL methods, applying simple augmentation in the MIM network (crop+flip&none) or target view (none&crop+flip) reduces performance, indicating that CRFR-P masking introduces sufficient spatial regularization and that preserving target representations from original faces aids robustness. **3) Loss for ID Network** Pretraining with asymmetric negative cosine similarity (NCS) *i.e.* Eq. (4) consistently outperforms the widely used InfoNCE, as the latter pushes different real faces (negative samples) apart that may not be suitable for face security tasks. Besides, our SimSiam-like [15] NCS proves more effective than BYOL-like [36] MSE.

Effect of Data Scaling As expected, pretraining FSFM on a larger dataset yields substantial gains, which suggests that incorporating more diverse real faces in open-ended environments can further improve generalization.

4.6. Qualitative analysis

To illustrate the superiority of the facial features learned by FSFM, we visualize GradCAM [86] activation maps for detecting forgery and spoofing, compared to Sup(IN) and MAE baselines. **1) DfD** In Fig. 4 (a), FSFM heatmaps more accurately identify forgery-relevant artifacts in FF++ [84], *e.g.*, mouth-modified F2F and NT. **2) FAS** In Fig. 4 (b), FSFM predominantly captures spoof-specific clues in the MCIO cross-domain testings: high-frequency paper textures (M-Paper), photo cut edges (C-Photo), inconsistent reflections between facial regions (I-Print), and moiré patterns in video (O-Replay). These visualizations show that FSFM effectively responds to anomalies diverging from the suggested 3C in real/live faces, shedding light on improving the generalization of face security tasks.

5. Conclusion

In this work, we propose a self-supervised pretraining framework to learn fundamental and general facial representations of real faces, FSFM. We leverage the synergy between masked image modeling and instance discrimination to empower both local and global perception, promoting intra-region consistency, inter-region coherency, and local-to-global correspondence. We show that our FSFM transfers better than previous pretrained models on several face security tasks, including cross-dataset deepfake detection, cross-domain face anti-spoofing, and unseen diffusion face forgery detection. Notably, as a vanilla ViT, our model surpasses SOTA task-specific methods on generalization performance. Finally, we hope that our work can contribute to the face security-related research.

References

- [1] Mahmoud Assran, Mathilde Caron, Ishan Misra, Piotr Bojanowski, Florian Bordes, Pascal Vincent, Armand Joulin, Mike Rabbat, and Nicolas Ballas. Masked siamese networks for label-efficient learning. In *European Conference on Computer Vision*, pages 456–473. Springer, 2022. 2, 3
- [2] Mahmoud Assran, Quentin Duval, Ishan Misra, Piotr Bojanowski, Pascal Vincent, Michael Rabbat, Yann LeCun, and Nicolas Ballas. Self-supervised learning from images with a joint-embedding predictive architecture. In *Proceedings of the IEEE/CVF Conference on Computer Vision and Pattern Recognition*, pages 15619–15629, 2023. 1, 2
- [3] Weiming Bai, Yufan Liu, Zhipeng Zhang, Bing Li, and Weiming Hu. Aunet: Learning relations between action units for face forgery detection. In *Proceedings of the IEEE/CVF Conference on Computer Vision and Pattern Recognition*, pages 24709–24719, 2023. 1, 6
- [4] Yutong Bai, Zeyu Wang, Junfei Xiao, Chen Wei, Huiyu Wang, Alan L Yuille, Yuyin Zhou, and Cihang Xie. Masked autoencoders enable efficient knowledge distillers. In *Proceedings of the IEEE/CVF conference on computer vision and pattern recognition*, pages 24256–24265, 2023. 2, 3
- [5] Hangbo Bao, Li Dong, Songhao Piao, and Furu Wei. Beit: Bert pre-training of image transformers. *arXiv preprint arXiv:2106.08254*, 2021. 1, 2
- [6] Zinelabinde Boulkenafet, Jukka Komulainen, Lei Li, Xiaoyi Feng, and Abdenour Hadid. Oulu-npu: A mobile face presentation attack database with real-world variations. In *2017 12th IEEE international conference on automatic face & gesture recognition (FG 2017)*, pages 612–618. IEEE, 2017. 7
- [7] Adrian Bulat, Shiyang Cheng, Jing Yang, Andrew Garrett, Enrique Sanchez, and Georgios Tzimiropoulos. Pre-training strategies and datasets for facial representation learning. In *European Conference on Computer Vision*, pages 107–125. Springer, 2022. 1, 2, 3
- [8] Zhixi Cai, Shreya Ghosh, Kalin Stefanov, Abhinav Dhall, Jianfei Cai, Hamid Rezatofighi, Reza Haffari, and Munawar Hayat. Marlin: Masked autoencoder for facial video representation learning. In *Proceedings of the IEEE/CVF conference on computer vision and pattern recognition*, pages 1493–1504, 2023. 2, 3, 4, 8
- [9] Junyi Cao, Chao Ma, Taiping Yao, Shen Chen, Shouhong Ding, and Xiaokang Yang. End-to-end reconstruction-classification learning for face forgery detection. In *Proceedings of the IEEE/CVF Conference on Computer Vision and Pattern Recognition*, pages 4113–4122, 2022. 6
- [10] Qiong Cao, Li Shen, Weidi Xie, Omkar M Parkhi, and Andrew Zisserman. Vggface2: A dataset for recognising faces across pose and age. In *2018 13th IEEE international conference on automatic face & gesture recognition (FG 2018)*, pages 67–74. IEEE, 2018. 5, 4
- [11] Mathilde Caron, Hugo Touvron, Ishan Misra, Hervé Jégou, Julien Mairal, Piotr Bojanowski, and Armand Joulin. Emerging properties in self-supervised vision transformers. In *Proceedings of the IEEE/CVF international conference on computer vision*, pages 9650–9660, 2021. 1, 2, 5, 6, 7, 4
- [12] Liang Chen, Yong Zhang, Yibing Song, Lingqiao Liu, and Jue Wang. Self-supervised learning of adversarial example: Towards good generalizations for deepfake detection. In *Proceedings of the IEEE/CVF conference on computer vision and pattern recognition*, pages 18710–18719, 2022. 2, 6
- [13] Liang Chen, Yong Zhang, Yibing Song, Jue Wang, and Lingqiao Liu. Ost: Improving generalization of deepfake detection via one-shot test-time training. *Advances in Neural Information Processing Systems*, 35:24597–24610, 2022. 2, 6
- [14] Ting Chen, Simon Kornblith, Mohammad Norouzi, and Geoffrey Hinton. A simple framework for contrastive learning of visual representations. In *International conference on machine learning*, pages 1597–1607. PMLR, 2020. 1, 2, 4
- [15] Xinlei Chen and Kaiming He. Exploring simple siamese representation learning. In *Proceedings of the IEEE/CVF conference on computer vision and pattern recognition*, pages 15750–15758, 2021. 1, 2, 5, 8, 4
- [16] Xinlei Chen, Saining Xie, and Kaiming He. An empirical study of training self-supervised vision transformers. In *Proceedings of the IEEE/CVF international conference on computer vision*, pages 9640–9649, 2021. 1, 2, 5, 4
- [17] Xiaokang Chen, Mingyu Ding, Xiaodi Wang, Ying Xin, Shentong Mo, Yunhao Wang, Shumin Han, Ping Luo, Gang Zeng, and Jingdong Wang. Context autoencoder for self-supervised representation learning. *International Journal of Computer Vision*, 132(1):208–223, 2024. 1, 2, 3
- [18] Harry Cheng, Yangyang Guo, Tianyi Wang, Liqiang Nie, and Mohan Kankanhalli. Diffusion facial forgery detection. In *Proceedings of the 32nd ACM International Conference on Multimedia*, page 5939–5948, New York, NY, USA, 2024. Association for Computing Machinery. 5
- [19] Harry Cheng, Yangyang Guo, Tianyi Wang, Liqiang Nie, and Mohan Kankanhalli. Diffusion facial forgery detection. *arXiv preprint arXiv:2401.15859*, 2024. 7, 6
- [20] Ivana Chingovska, André Anjos, and Sébastien Marcel. On the effectiveness of local binary patterns in face anti-spoofing. In *2012 BIOSIG-proceedings of the international*

- conference of biometrics special interest group (BIOSIG), pages 1–7. IEEE, 2012. 7
- [21] Jongwook Choi, Taehoon Kim, Yonghyun Jeong, Seungryul Baek, and Jongwon Choi. Exploiting style latent flows for generalizing deepfake video detection. In *Proceedings of the IEEE/CVF Conference on Computer Vision and Pattern Recognition*, pages 1133–1143, 2024. 1, 6
- [22] François Chollet. Xception: Deep learning with depthwise separable convolutions. In *Proceedings of the IEEE conference on computer vision and pattern recognition*, pages 1251–1258, 2017. 1, 6, 4
- [23] Davide Cozzolino, Giovanni Poggi, Riccardo Corvi, Matthias Nießner, and Luisa Verdoliva. Raising the bar of ai-generated image detection with clip. In *Proceedings of the IEEE/CVF Conference on Computer Vision and Pattern Recognition*, pages 4356–4366, 2024. 6
- [24] Debayan Deb, Xiaoming Liu, and Anil K Jain. Unified detection of digital and physical face attacks. In *2023 IEEE 17th International Conference on Automatic Face and Gesture Recognition (FG)*, pages 1–8. IEEE, 2023. 2
- [25] Jia Deng, Wei Dong, Richard Socher, Li-Jia Li, Kai Li, and Li Fei-Fei. Imagenet: A large-scale hierarchical image database. In *2009 IEEE conference on computer vision and pattern recognition*, pages 248–255. Ieee, 2009. 1, 4, 5
- [26] B Dolhansky. The dee pfake detection challenge (dfdc) pre view dataset. *arXiv preprint arXiv:1910.08854*, 2019. 6, 5
- [27] Brian Dolhansky, Joanna Bitton, Ben Pfau, Jikuo Lu, Russ Howes, Menglin Wang, and Cristian Canton Ferrer. The deepfake detection challenge (dfdc) dataset. *arXiv preprint arXiv:2006.07397*, 2020. 6, 5
- [28] Alexey Dosovitskiy, Lucas Beyer, Alexander Kolesnikov, Dirk Weissenborn, Xiaohua Zhai, Thomas Unterthiner, Mostafa Dehghani, Matthias Minderer, Georg Heigold, Sylvain Gelly, et al. An image is worth 16x16 words: Transformers for image recognition at scale. In *International Conference on Learning Representations*, 2020. 1, 6, 7, 4, 5
- [29] Paul Ekman and Wallace V Friesen. Facial action coding system. *Environmental Psychology & Nonverbal Behavior*, 1978. 3
- [30] Alexandre Eymaël, Renaud Vandeghen, Anthony Cioppa, Silvio Giancola, Bernard Ghanem, and Marc Van Droogenbroeck. Efficient image pre-training with siamese cropped masked autoencoders. *arXiv preprint arXiv:2403.17823*, 2024. 2
- [31] Chao Feng, Ziyang Chen, and Andrew Owens. Self-supervised video forensics by audio-visual anomaly detection. In *Proceedings of the IEEE/CVF Conference on Computer Vision and Pattern Recognition*, pages 10491–10503, 2023. 2
- [32] Zheng Gao and Ioannis Patras. Self-supervised facial representation learning with facial region awareness. In *Proceedings of the IEEE/CVF Conference on Computer Vision and Pattern Recognition*, pages 2081–2092, 2024. 2, 3
- [33] Anjith George and Sébastien Marcel. On the effectiveness of vision transformers for zero-shot face anti-spoofing. In *2021 IEEE International Joint Conference on Biometrics (IJCB)*, pages 1–8. IEEE, 2021. 4
- [34] Ian Goodfellow, Jean Pouget-Abadie, Mehdi Mirza, Bing Xu, David Warde-Farley, Sherjil Ozair, Aaron Courville, and Yoshua Bengio. Generative adversarial nets. *Advances in neural information processing systems*, 27, 2014. 1
- [35] P Goyal. Accurate, large minibatch sg d: training imagenet in 1 hour. *arXiv preprint arXiv:1706.02677*, 2017. 5
- [36] Jean-Bastien Grill, Florian Strub, Florent Altché, Corentin Tallec, Pierre Richemond, Elena Buchatskaya, Carl Doersch, Bernardo Avila Pires, Zhaohan Guo, Mohammad Gheshlaghi Azar, et al. Bootstrap your own latent-a new approach to self-supervised learning. *Advances in neural information processing systems*, 33:21271–21284, 2020. 1, 2, 5, 6, 8, 4
- [37] Qiqi Gu, Shen Chen, Taiping Yao, Yang Chen, Shouhong Ding, and Ran Yi. Exploiting fine-grained face forgery clues via progressive enhancement learning. In *Proceedings of the AAAI Conference on Artificial Intelligence*, pages 735–743, 2022. 6
- [38] Zhihao Gu, Taiping Yao, Yang Chen, Shouhong Ding, and Lizhuang Ma. Hierarchical contrastive inconsistency learning for deepfake video detection. In *European Conference on Computer Vision*, pages 596–613. Springer, 2022. 6
- [39] Jiabao Guo, Huan Liu, Yizhi Luo, Xueli Hu, Hang Zou, Yuan Zhang, Hui Liu, and Bo Zhao. Style-conditional prompt token learning for generalizable face anti-spoofing. In *Proceedings of the 32nd ACM International Conference on Multimedia*, pages 994–1003, 2024. 6
- [40] Ying Guo, Cheng Zhen, and Pengfei Yan. Controllable guide-space for generalizable face forgery detection. In *Proceedings of the IEEE/CVF International Conference on Computer Vision*, pages 20818–20827, 2023. 6
- [41] Alexandros Haliassos, Rodrigo Mira, Stavros Petridis, and Maja Pantic. Leveraging real talking faces via self-supervision for robust forgery detection. In *Proceedings of the IEEE/CVF Conference on Computer Vision and Pattern Recognition*, pages 14950–14962, 2022. 2, 6
- [42] James V Haxby, Elizabeth A Hoffman, and M Ida Gobbini. The distributed human neural system for face perception. *Trends in cognitive sciences*, 4(6):223–233, 2000. 3
- [43] Kaiming He, Xiangyu Zhang, Shaoqing Ren, and Jian Sun. Deep residual learning for image recognition. In *Proceedings of the IEEE conference on computer vision and pattern recognition*, pages 770–778, 2016. 1
- [44] Kaiming He, Haoqi Fan, Yuxin Wu, Saining Xie, and Ross Girshick. Momentum contrast for unsupervised visual representation learning. In *Proceedings of the IEEE/CVF conference on computer vision and pattern recognition*, pages 9729–9738, 2020. 1, 2, 4
- [45] Kaiming He, Xinlei Chen, Saining Xie, Yanghao Li, Piotr Dollár, and Ross Girshick. Masked autoencoders are scalable vision learners. In *Proceedings of the IEEE/CVF conference on computer vision and pattern recognition*, pages 16000–16009, 2022. 1, 2, 3, 4, 5, 6, 7
- [46] Jefferson Hernandez, Ruben Villegas, and Vicente Ordonez. Vic-mae: Self-supervised representation learning from images and video with contrastive masked autoencoders. In *European Conference on Computer Vision*, pages 444–463. Springer, 2025. 1, 2

- [47] Jonathan Ho, Ajay Jain, and Pieter Abbeel. Denoising diffusion probabilistic models. *Advances in neural information processing systems*, 33:6840–6851, 2020. 1
- [48] Cheng-Yao Hong, Yen-Chi Hsu, and Tyng-Luh Liu. Contrastive learning for deepfake classification and localization via multi-label ranking. In *Proceedings of the IEEE/CVF Conference on Computer Vision and Pattern Recognition*, pages 17627–17637, 2024. 1, 6
- [49] Zejiang Hou, Fei Sun, Yen-Kuang Chen, Yuan Xie, and Sun-Yuan Kung. Milan: Masked image pretraining on language assisted representation. *arXiv preprint arXiv:2208.06049*, 2022. 3
- [50] Chengyang Hu, Ke-Yue Zhang, Taiping Yao, Shouhong Ding, and Lizhuang Ma. Rethinking generalizable face anti-spoofing via hierarchical prototype-guided distribution refinement in hyperbolic space. In *Proceedings of the IEEE/CVF Conference on Computer Vision and Pattern Recognition*, pages 1032–1041, 2024. 1, 7
- [51] Juan Hu, Xin Liao, Jinwen Liang, Wenbo Zhou, and Zheng Qin. Finfer: Frame inference-based deepfake detection for high-visual-quality videos. In *Proceedings of the AAAI conference on artificial intelligence*, pages 951–959, 2022. 6
- [52] Xueli Hu, Huan Liu, Haocheng Yuan, Zhiyang Fu, Yizhi Luo, Ning Zhang, Hang Zou, Jianwen Gan, and Yuan Zhang. Fine-grained prompt learning for face anti-spoofing. In *Proceedings of the 32nd ACM International Conference on Multimedia*, pages 7619–7628, 2024. 6
- [53] Baojin Huang, Zhongyuan Wang, Jifan Yang, Jiabin Ai, Qin Zou, Qian Wang, and Dengpan Ye. Implicit identity driven deepfake face swapping detection. In *Proceedings of the IEEE/CVF conference on computer vision and pattern recognition*, pages 4490–4499, 2023. 6
- [54] Hsin-Ping Huang, Deqing Sun, Yaojie Liu, Wen-Sheng Chu, Taihong Xiao, Jinwei Yuan, Hartwig Adam, and Ming-Hsuan Yang. Adaptive transformers for robust few-shot cross-domain face anti-spoofing. In *European conference on computer vision*, pages 37–54. Springer, 2022. 7, 4, 5
- [55] Zhicheng Huang, Xiaojie Jin, Chengze Lu, Qibin Hou, Ming-Ming Cheng, Dongmei Fu, Xiaohui Shen, and Jiashi Feng. Contrastive masked autoencoders are stronger vision learners. *IEEE Transactions on Pattern Analysis and Machine Intelligence*, 2023. 1, 2, 3, 4
- [56] Yunpei Jia, Jie Zhang, Shiguang Shan, and Xilin Chen. Single-side domain generalization for face anti-spoofing. In *Proceedings of the IEEE/CVF Conference on Computer Vision and Pattern Recognition*, pages 8484–8493, 2020. 7
- [57] Ioannis Kakogeorgiou, Spyros Gidaris, Bill Psomas, Yannis Avrithis, Andrei Bursuc, Konstantinos Karantzas, and Nikos Komodakis. What to hide from your students: Attention-guided masked image modeling. In *European Conference on Computer Vision*, pages 300–318. Springer, 2022. 2, 3
- [58] Sohail Ahmed Khan and Duc-Tien Dang-Nguyen. Clipping the deception: Adapting vision-language models for universal deepfake detection. In *Proceedings of the 2024 International Conference on Multimedia Retrieval*, pages 1006–1015, 2024. 6
- [59] Davis E King. Dlib-ml: A machine learning toolkit. *The Journal of Machine Learning Research*, 10:1755–1758, 2009. 5
- [60] Diederik P Kingma. Auto-encoding variational bayes. *arXiv preprint arXiv:1312.6114*, 2013. 1
- [61] Nicolas Larue, Ngoc-Son Vu, Vitomir Struc, Peter Peer, and Vassilis Christophides. Seeable: Soft discrepancies and bounded contrastive learning for exposing deepfakes. In *Proceedings of the IEEE/CVF International Conference on Computer Vision*, pages 21011–21021, 2023. 2, 6
- [62] Binh M Le and Simon S Woo. Gradient alignment for cross-domain face anti-spoofing. In *Proceedings of the IEEE/CVF Conference on Computer Vision and Pattern Recognition*, pages 188–199, 2024. 1, 7
- [63] Gang Li, Heliang Zheng, Daqing Liu, Chaoyue Wang, Bing Su, and Changwen Zheng. Semmae: Semantic-guided masking for learning masked autoencoders. *Advances in Neural Information Processing Systems*, 35:14290–14302, 2022. 2, 3
- [64] Tianhong Li, Huiwen Chang, Shlok Mishra, Han Zhang, Dina Katabi, and Dilip Krishnan. Mage: Masked generative encoder to unify representation learning and image synthesis. In *Proceedings of the IEEE/CVF Conference on Computer Vision and Pattern Recognition*, pages 2142–2152, 2023. 2, 3, 4
- [65] Yuezun Li, Xin Yang, Pu Sun, Honggang Qi, and Siwei Lyu. Celeb-df: A large-scale challenging dataset for deepfake forensics. In *Proceedings of the IEEE/CVF conference on computer vision and pattern recognition*, pages 3207–3216, 2020. 6, 5
- [66] Yong Li, Jiabei Zeng, and Shiguang Shan. Learning representations for facial actions from unlabeled videos. *IEEE Transactions on Pattern Analysis and Machine Intelligence*, 44(1):302–317, 2020. 2
- [67] Chen-Hao Liao, Wen-Cheng Chen, Hsuan-Tung Liu, Yi-Ren Yeh, Min-Chun Hu, and Chu-Song Chen. Domain invariant vision transformer learning for face anti-spoofing. In *Proceedings of the IEEE/CVF Winter Conference on Applications of Computer Vision*, pages 6098–6107, 2023. 7, 4
- [68] Li Lin, Irene Amerini, Xin Wang, Shu Hu, et al. Robust clip-based detector for exposing diffusion model-generated images. *arXiv preprint arXiv:2404.12908*, 2024. 6
- [69] Aajian Liu, Shuai Xue, Jianwen Gan, Jun Wan, Yanyan Liang, Jiankang Deng, Sergio Escalera, and Zhen Lei. Cfpl-fas: Class free prompt learning for generalizable face anti-spoofing. In *Proceedings of the IEEE/CVF Conference on Computer Vision and Pattern Recognition*, pages 222–232, 2024. 6
- [70] Shice Liu, Shitao Lu, Hongyi Xu, Jing Yang, Shouhong Ding, and Lizhuang Ma. Feature generation and hypothesis verification for reliable face anti-spoofing. In *Proceedings of the AAAI Conference on Artificial Intelligence*, pages 1782–1791, 2022. 7
- [71] Si-Qi Liu, Qirui Wang, and Pong C. Yuen. Bottom-up domain prompt tuning for generalized face anti-spoofing. In *Computer Vision – ECCV 2024*, pages 170–187, Cham, 2025. Springer Nature Switzerland. 6

- [72] Yuchen Liu, Yabo Chen, Wenrui Dai, Mengran Gou, Chun-Ting Huang, and Hongkai Xiong. Source-free domain adaptation with contrastive domain alignment and self-supervised exploration for face anti-spoofing. In *European Conference on Computer Vision*, pages 511–528. Springer, 2022. 2
- [73] Yuchen Liu, Yabo Chen, Mengran Gou, Chun-Ting Huang, Yaoming Wang, Wenrui Dai, and Hongkai Xiong. Towards unsupervised domain generalization for face anti-spoofing. In *Proceedings of the IEEE/CVF International Conference on Computer Vision*, pages 20654–20664, 2023. 2, 7
- [74] Yuanyuan Liu, Wenbin Wang, Yibing Zhan, Shaoze Feng, Kejun Liu, and Zhe Chen. Pose-disentangled contrastive learning for self-supervised facial representation. In *Proceedings of the IEEE/CVF Conference on Computer Vision and Pattern Recognition*, pages 9717–9728, 2023. 2, 3
- [75] I Loshchilov. Decoupled weight decay regularization. *arXiv preprint arXiv:1711.05101*, 2017. 5
- [76] Ilya Loshchilov and Frank Hutter. Sgdr: Stochastic gradient descent with warm restarts. *arXiv preprint arXiv:1608.03983*, 2016. 5
- [77] Dat Nguyen, Nesryne Mejri, Inder Pal Singh, Polina Kuleshova, Marcella Astrid, Anis Kacem, Enjie Ghorbel, and Djamila Aouada. Laa-net: Localized artifact attention network for quality-agnostic and generalizable deepfake detection. In *Proceedings of the IEEE/CVF Conference on Computer Vision and Pattern Recognition*, pages 17395–17405, 2024. 1, 6
- [78] Duy-Kien Nguyen, Vaibhav Aggarwal, Yanghao Li, Martin R Oswald, Alexander Kirillov, Cees GM Snoek, and Xinlei Chen. R-mae: Regions meet masked autoencoders. *arXiv preprint arXiv:2306.05411*, 2023. 2
- [79] Xuan-Bac Nguyen, Chi Nhan Duong, Xin Li, Susan Gauch, Han-Seok Seo, and Khoa Luu. Micron-bert: Bert-based facial micro-expression recognition. In *Proceedings of the IEEE/CVF Conference on Computer Vision and Pattern Recognition*, pages 1482–1492, 2023. 2
- [80] Aaron van den Oord, Yazhe Li, and Oriol Vinyals. Representation learning with contrastive predictive coding. *arXiv preprint arXiv:1807.03748*, 2018. 4
- [81] Utku Ozbek, Hyun Jung Lee, Beril Boga, Esla Timothy Anzaku, Ho min Park, Arnout Van Messem, Wesley De Neve, and Joris Vankerschaver. Know your self-supervised learning: A survey on image-based generative and discriminative training. *Transactions on Machine Learning Research*, 2023. Survey Certification. 1, 2
- [82] Namuk Park, Wonjae Kim, Byeongho Heo, Taekyung Kim, and Sangdoon Yun. What do self-supervised vision transformers learn? *arXiv preprint arXiv:2305.00729*, 2023. 1, 2
- [83] Alec Radford, Jong Wook Kim, Chris Hallacy, Aditya Ramesh, Gabriel Goh, Sandhini Agarwal, Girish Sastry, Amanda Askell, Pamela Mishkin, Jack Clark, et al. Learning transferable visual models from natural language supervision. In *International conference on machine learning*, pages 8748–8763. PMLR, 2021. 4, 5, 6
- [84] Andreas Rossler, Davide Cozzolino, Luisa Verdoliva, Christian Riess, Justus Thies, and Matthias Nießner. Face-forensics++: Learning to detect manipulated facial images. In *Proceedings of the IEEE/CVF international conference on computer vision*, pages 1–11, 2019. 6, 7, 8, 1, 5
- [85] James A Russell and José Miguel Fernandez-Dols. *The psychology of facial expression*. Cambridge university press, 1997. 3
- [86] Ramprasaath R Selvaraju, Michael Cogswell, Abhishek Das, Ramakrishna Vedantam, Devi Parikh, and Dhruv Batra. Grad-cam: Visual explanations from deep networks via gradient-based localization. In *Proceedings of the IEEE international conference on computer vision*, pages 618–626, 2017. 8
- [87] Rui Shao, Xiangyuan Lan, Jiawei Li, and Pong C Yuen. Multi-adversarial discriminative deep domain generalization for face presentation attack detection. In *Proceedings of the IEEE/CVF conference on computer vision and pattern recognition*, pages 10023–10031, 2019. 7
- [88] Yuge Shi, N Siddharth, Philip Torr, and Adam R Kosiorek. Adversarial masking for self-supervised learning. In *International Conference on Machine Learning*, pages 20026–20040. PMLR, 2022. 2, 3
- [89] Kaede Shiohara and Toshihiko Yamasaki. Detecting deepfakes with self-blended images. In *Proceedings of the IEEE/CVF Conference on Computer Vision and Pattern Recognition*, pages 18720–18729, 2022. 1, 2, 6
- [90] Stefan Smeu, Elisabeta Oneata, and Dan Oneata. De-clip: Decoding clip representations for deepfake localization. *arXiv preprint arXiv:2409.08849*, 2024. 6
- [91] Koushik Srivatsan, Muzammal Naseer, and Karthik Nandakumar. Flip: Cross-domain face anti-spoofing with language guidance. In *Proceedings of the IEEE/CVF International Conference on Computer Vision*, pages 19685–19696, 2023. 6
- [92] Yiyou Sun, Yaojie Liu, Xiaoming Liu, Yixuan Li, and Wen-Sheng Chu. Rethinking domain generalization for face anti-spoofing: Separability and alignment. In *Proceedings of the IEEE/CVF conference on computer vision and pattern recognition*, pages 24563–24574, 2023. 1, 7
- [93] Zhonglin Sun, Chen Feng, Ioannis Patras, and Georgios Tzimiropoulos. Lafs: Landmark-based facial self-supervised learning for face recognition. In *Proceedings of the IEEE/CVF Conference on Computer Vision and Pattern Recognition*, pages 1639–1649, 2024. 2
- [94] Chuangchuang Tan, Renshuai Tao, Huan Liu, Guanghua Gu, Baoyuan Wu, Yao Zhao, and Yunchao Wei. C2p-clip: Injecting category common prompt in clip to enhance generalization in deepfake detection. *arXiv preprint arXiv:2408.09647*, 2024. 6
- [95] Mingxing Tan. Efficientnet: Rethinking model scaling for convolutional neural networks. *arXiv preprint arXiv:1905.11946*, 2019. 1, 6, 4
- [96] Chenxin Tao, Xizhou Zhu, Weijie Su, Gao Huang, Bin Li, Jie Zhou, Yu Qiao, Xiaogang Wang, and Jifeng Dai. Siamese image modeling for self-supervised vision representation learning. In *Proceedings of the IEEE/CVF Conference on Computer Vision and Pattern Recognition*, pages 2132–2141, 2023. 1, 2, 3

- [97] Siddharth Tourani, Ahmed Alwheibi, Arif Mahmood, and Muhammad Haris Khan. Pose-guided self-training with two-stage clustering for unsupervised landmark discovery. In *Proceedings of the IEEE/CVF Conference on Computer Vision and Pattern Recognition*, pages 23041–23051, 2024. 2
- [98] Ashish Vaswani, Noam Shazeer, Niki Parmar, Jakob Uszkoreit, Llion Jones, Aidan N Gomez, Łukasz Kaiser, and Illia Polosukhin. Attention is all you need. *Advances in neural information processing systems*, 30, 2017. 1
- [99] Chien-Yi Wang, Yu-Ding Lu, Shang-Ta Yang, and Shang-Hong Lai. Patchnet: A simple face anti-spoofing framework via fine-grained patch recognition. In *Proceedings of the IEEE/CVF Conference on Computer Vision and Pattern Recognition*, pages 20281–20290, 2022. 7
- [100] Hao Wang, Min Li, Yangyang Song, Youjian Zhang, and Liying Chi. Ucol: unsupervised learning of discriminative facial representations via uncertainty-aware contrast. In *Proceedings of the AAAI Conference on Artificial Intelligence*, pages 2510–2518, 2023. 2
- [101] Haochen Wang, Kaiyou Song, Junsong Fan, Yuxi Wang, Jin Xie, and Zhaoxiang Zhang. Hard patches mining for masked image modeling. In *Proceedings of the IEEE/CVF Conference on Computer Vision and Pattern Recognition*, pages 10375–10385, 2023. 2, 3
- [102] Tianyi Wang and Kam Pui Chow. Noise based deepfake detection via multi-head relative-interaction. In *Proceedings of the AAAI Conference on Artificial Intelligence*, pages 14548–14556, 2023. 6
- [103] Yue Wang, Jinlong Peng, Jiangning Zhang, Ran Yi, Liang Liu, Yabiao Wang, and Chengjie Wang. Toward high quality facial representation learning. In *Proceedings of the 31st ACM International Conference on Multimedia*, pages 5048–5058, 2023. 3, 6, 7, 4, 5
- [104] Yuan Wang, Kun Yu, Chen Chen, Xiyuan Hu, and Silong Peng. Dynamic graph learning with content-guided spatial-frequency relation reasoning for deepfake detection. In *Proceedings of the IEEE/CVF Conference on Computer Vision and Pattern Recognition*, pages 7278–7287, 2023. 6
- [105] Zhuo Wang, Qiangchang Wang, Weihong Deng, and Guodong Guo. Face anti-spoofing using transformers with relation-aware mechanism. *IEEE Transactions on Biometrics, Behavior, and Identity Science*, 4(3):439–450, 2022. 4
- [106] Zhuo Wang, Qiangchang Wang, Weihong Deng, and Guodong Guo. Learning multi-granularity temporal characteristics for face anti-spoofing. *IEEE Transactions on Information Forensics and Security*, 17:1254–1269, 2022. 7, 4
- [107] Zhuo Wang, Zezheng Wang, Zitong Yu, Weihong Deng, Jiahong Li, Tingting Gao, and Zhongyuan Wang. Domain generalization via shuffled style assembly for face anti-spoofing. In *Proceedings of the IEEE/CVF conference on computer vision and pattern recognition*, pages 4123–4133, 2022. 7
- [108] Zhendong Wang, Jianmin Bao, Wengang Zhou, Weilun Wang, and Houqiang Li. Altfreezing for more general video face forgery detection. In *Proceedings of the IEEE/CVF conference on computer vision and pattern recognition*, pages 4129–4138, 2023. 1
- [109] Chen Wei, Haoqi Fan, Saining Xie, Chao-Yuan Wu, Alan Yuille, and Christoph Feichtenhofer. Masked feature prediction for self-supervised visual pre-training. In *Proceedings of the IEEE/CVF Conference on Computer Vision and Pattern Recognition*, pages 14668–14678, 2022. 2
- [110] Di Wen, Hu Han, and Anil K Jain. Face spoof detection with image distortion analysis. *IEEE Transactions on Information Forensics and Security*, 10(4):746–761, 2015. 7
- [111] Lior Wolf, Tal Hassner, and Itay Maoz. Face recognition in unconstrained videos with matched background similarity. In *CVPR 2011*, pages 529–534. IEEE, 2011. 8
- [112] Yanqi Wu, Xue Song, Jingjing Chen, and Yu-Gang Jiang. Generalizing face forgery detection via uncertainty learning. In *Proceedings of the 31st ACM International Conference on Multimedia*, pages 1759–1767, 2023. 6
- [113] Ruiyang Xia, Dawei Zhou, Decheng Liu, Lin Yuan, Shuodi Wang, Jie Li, Nannan Wang, and Xinbo Gao. Advancing generalized deepfake detector with forgery perception guidance. In *ACM Multimedia 2024*, 2024. 1, 6
- [114] Zhenda Xie, Zheng Zhang, Yue Cao, Yutong Lin, Jianmin Bao, Zhuliang Yao, Qi Dai, and Han Hu. Simmim: A simple framework for masked image modeling. In *Proceedings of the IEEE/CVF conference on computer vision and pattern recognition*, pages 9653–9663, 2022. 1, 2, 3
- [115] Zhenda Xie, Zigang Geng, Jingcheng Hu, Zheng Zhang, Han Hu, and Yue Cao. Revealing the dark secrets of masked image modeling. In *Proceedings of the IEEE/CVF conference on computer vision and pattern recognition*, pages 14475–14485, 2023. 1
- [116] Yuting Xu, Jian Liang, Gengyun Jia, Ziming Yang, Yanhao Zhang, and Ran He. Tall: Thumbnail layout for deepfake video detection. In *Proceedings of the IEEE/CVF international conference on computer vision*, pages 22658–22668, 2023. 6
- [117] Zhiyuan Yan, Yong Zhang, Yanbo Fan, and Baoyuan Wu. Ucf: Uncovering common features for generalizable deepfake detection. In *Proceedings of the IEEE/CVF International Conference on Computer Vision*, pages 22412–22423, 2023. 6
- [118] Zhiyuan Yan, Yuhao Luo, Siwei Lyu, Qingshan Liu, and Baoyuan Wu. Transcending forgery specificity with latent space augmentation for generalizable deepfake detection. In *Proceedings of the IEEE/CVF Conference on Computer Vision and Pattern Recognition*, pages 8984–8994, 2024. 6
- [119] Kun Yi, Yixiao Ge, Xiaotong Li, Shusheng Yang, Dian Li, Jianping Wu, Ying Shan, and Xiaohu Qie. Masked image modeling with denoising contrast. *arXiv preprint arXiv:2205.09616*, 2022. 2, 3, 4
- [120] Zitong Yu, Rizhao Cai, Yawen Cui, Xin Liu, Yongjian Hu, and Alex C Kot. Rethinking vision transformer and masked autoencoder in multimodal face anti-spoofing. *International Journal of Computer Vision*, pages 1–22, 2024. 7
- [121] Zitong Yu, Rizhao Cai, Zhi Li, Wenhan Yang, Jingang Shi, and Alex C Kot. Benchmarking joint face spoofing and

- forgery detection with visual and physiological cues. *IEEE Transactions on Dependable and Secure Computing*, 2024. 2
- [122] Haocheng Yuan, Ajian Liu, Junze Zheng, Jun Wan, Jiankang Deng, Sergio Escalera, Hugo Jair Escalante, Isabelle Guyon, and Zhen Lei. Unified physical-digital attack detection challenge. In *Proceedings of the IEEE/CVF Conference on Computer Vision and Pattern Recognition*, pages 919–929, 2024. 2
- [123] Daichi Zhang, Zihao Xiao, Shikun Li, Fanzhao Lin, Jianmin Li, and Shiming Ge. Learning natural consistency representation for face forgery video detection. *arXiv preprint arXiv:2407.10550*, 2024. 2, 6
- [124] Yuanhan Zhang, Zhenfei Yin, Yidong Li, Guojun Yin, Junjie Yan, Jing Shao, and Ziwei Liu. Celeba-spoof: Large-scale face anti-spoofing dataset with rich annotations. In *Computer Vision—ECCV 2020: 16th European Conference, Glasgow, UK, August 23–28, 2020, Proceedings, Part XII 16*, pages 70–85. Springer, 2020. 7, 5
- [125] Yaning Zhang, Tianyi Wang, Zitong Yu, Zan Gao, Linlin Shen, and Shengyong Chen. Mfclip: Multi-modal fine-grained clip for generalizable diffusion face forgery detection. *arXiv preprint arXiv:2409.09724*, 2024. 6
- [126] Zhiwei Zhang, Junjie Yan, Sifei Liu, Zhen Lei, Dong Yi, and Stan Z Li. A face antispoofing database with diverse attacks. In *2012 5th IAPR international conference on Biometrics (ICB)*, pages 26–31. IEEE, 2012. 7
- [127] Hanqing Zhao, Wenbo Zhou, Dongdong Chen, Weiming Zhang, and Nenghai Yu. Self-supervised transformer for deepfake detection. *arXiv preprint arXiv:2203.01265*, 2022. 2
- [128] Zhiyu Zhao, Bingkun Huang, Sen Xing, Gangshan Wu, Yu Qiao, and Limin Wang. Asymmetric masked distillation for pre-training small foundation models. In *Proceedings of the IEEE/CVF Conference on Computer Vision and Pattern Recognition*, pages 18516–18526, 2024. 1, 2, 3
- [129] Tianyi Zheng, Bo Li, Shuang Wu, Ben Wan, Guodong Mu, Shice Liu, Shouhong Ding, and Jia Wang. Mfae: Masked frequency autoencoders for domain generalization face anti-spoofing. *IEEE Transactions on Information Forensics and Security*, 2024. 2
- [130] Yinglin Zheng, Hao Yang, Ting Zhang, Jianmin Bao, Dongdong Chen, Yangyu Huang, Lu Yuan, Dong Chen, Ming Zeng, and Fang Wen. General facial representation learning in a visual-linguistic manner. In *Proceedings of the IEEE/CVF conference on computer vision and pattern recognition*, pages 18697–18709, 2022. 1, 2, 3, 5
- [131] Jinghao Zhou, Chen Wei, Huiyu Wang, Wei Shen, Cihang Xie, Alan Yuille, and Tao Kong. ibot: Image bert pre-training with online tokenizer. *arXiv preprint arXiv:2111.07832*, 2021. 2, 3
- [132] Qianyu Zhou, Ke-Yue Zhang, Taiping Yao, Ran Yi, Shouhong Ding, and Lizhuang Ma. Adaptive mixture of experts learning for generalizable face anti-spoofing. In *Proceedings of the 30th ACM international conference on multimedia*, pages 6009–6018, 2022. 7
- [133] Qianyu Zhou, Ke-Yue Zhang, Taiping Yao, Xuequan Lu, Ran Yi, Shouhong Ding, and Lizhuang Ma. Instance-aware domain generalization for face anti-spoofing. In *Proceedings of the IEEE/CVF Conference on Computer Vision and Pattern Recognition*, pages 20453–20463, 2023. 1, 7
- [134] Qianyu Zhou, Ke-Yue Zhang, Taiping Yao, Xuequan Lu, Shouhong Ding, and Lizhuang Ma. Test-time domain generalization for face anti-spoofing. In *Proceedings of the IEEE/CVF Conference on Computer Vision and Pattern Recognition*, pages 175–187, 2024. 1, 7, 4, 5
- [135] Jie Zhu, Jiyang Qi, Mingyu Ding, Xiaokang Chen, Ping Luo, Xinggang Wang, Wenyu Liu, Leye Wang, and Jingdong Wang. Understanding self-supervised pretraining with part-aware representation learning. *Transactions on Machine Learning Research*, 2023. 1, 2, 6
- [136] Wanyu Zhuang, Qi Chu, Zhentao Tan, Qiankun Liu, Haojie Yuan, Changtao Miao, Zixiang Luo, and Nenghai Yu. Uia-vit: Unsupervised inconsistency-aware method based on vision transformer for face forgery detection. In *European conference on computer vision*, pages 391–407. Springer, 2022. 2, 6
- [137] Bojia Zi, Minghao Chang, Jingjing Chen, Xingjun Ma, and Yu-Gang Jiang. Wilddeepfake: A challenging real-world dataset for deepfake detection. In *Proceedings of the 28th ACM international conference on multimedia*, pages 2382–2390, 2020. 6, 5

FSFM: A Generalizable Face Security Foundation Model via Self-Supervised Facial Representation Learning

Supplementary Material

A. Overview

This supplementary material provides additional insights, details, and results supporting our FSFM framework, structured as follows:

- Facial Masking Strategies in MIM (Sec. B): We delve into the impact of different facial masking strategies on naive MAE, including quantitative and qualitative analyses of attention differences.
- Instance Discrimination in FSFM (Sec. C): We highlight the connections and distinctions between our method and prior works that also integrate ID (or Siamese encoder architecture) into MIM (or degraded input).
- Implementation Details (Sec. D): Detailed descriptions of hyperparameters, pretraining, and finetuning settings.
- Additional Results and Comparisons (Sec. E): Extended experiments comparing FSFM against other models, including ViT-based FAS and the base VLP model, CLIP.
- Ablations and Visualizations (Sec. F): Supplementary evidence validating FSFM’s ability to learn robust and transferable facial representations.

B. Revealing the secrets of facial masking strategies in MIM

In the main paper, we explore various facial masking strategies for masked image modeling (MIM) in FSFM, with additional visualizations provided in Fig. 5, and validate the effectiveness of CRFR-P masking through ablation studies on downstream face security tasks. However, a critical question remains: how do different facial masking strategies affect the MIM pretrained model or its learned representations of real faces?

To address this, we quantitatively and qualitatively analyze the properties of attention maps. Given that most MIM pretrained models, including ours, are built on the Vision Transformer (ViT) architecture [28], whose main component, the attention mechanism [98], is naturally interpretable [115]. Here, we adopt the naive MAE (FSFM without the ID network) and follow its settings [45] with ViT-B/16 as the encoder and a 75% masking ratio. We conduct self-supervised pretraining on real face images from FF++_o [84] (the default dataset for our ablations). We alter only the masking strategy, encompassing simple random masking, Fasking-I, FRP, CRFR-R, and CRFR-P, and we examine the following aspects of attention heads in the pretrained models: 1) mean attention distance to measure the flow of local and global facial information; 2) KL diver-

gence to investigate the diversity of attention; 3) visualized attention maps to uncover key regions of focus.

B.1. Local or global?

To explore whether the pretrained model attends to faces locally or globally, we calculate the mean attention distance [28] in each attention head across all blocks/layers, as shown in Fig. 6 (top). The model (MAE ViT-B/16 encoder) pretrained with simple random masking tends to focus on local information in the lower blocks and shifts toward global attention in the deeper blocks, similar to the supervised model [28]. Fasking-I primarily aggregates global information as the visible patches predominantly consist of broad backgrounds and skin. FRP also causes large mean attention distances, but they are slightly smaller than those of Fasking-I, mainly because visible patches in FRP are more evenly distributed across all facial regions. CRFR-R fully masks a facial region before applying random masking, which encourages attention to different regions. Consequently, CRFR-R has more global attention in the middle (3rd to 8th) blocks than the simple random masking counterparts. Compared with CRFR-R, CRFR-P masks the remaining regions proportionally instead of randomly, making the 1st block more global w.r.t. the more unmasked regions. Compared with FRP, CRFR-P fully masks a region before applying proportional masking, exposing more patches within other regions at the same masking ratio, thus leading to more local attention than FRP.

Overall, the model pretrained with CRFR-P exhibits well-distributed mean attention distances across all blocks, indicating a synergistic effect of FRP and CRFR-R, enabling appropriate attention to both local and global information.

B.2. Similar or different?

To assess whether the pretrained model focuses on similar or different tokens, we compute the Kullback-Leibler (KL) divergence between attention maps of each head across all blocks, following [115], as shown in Fig. 6 (bottom). As the visible patches are mostly background and skin, the model pretrained with Fasking-I aggregates similar tokens, leading to low KL divergence across all attention heads. Interestingly, we find that proportional masking reduces diversity among attention heads, likely due to its homogeneous presentation of visible tokens, *i.e.*, derived from each facial region. In contrast, covering a random facial region increases attention diversity, as evidenced by higher KL diver-

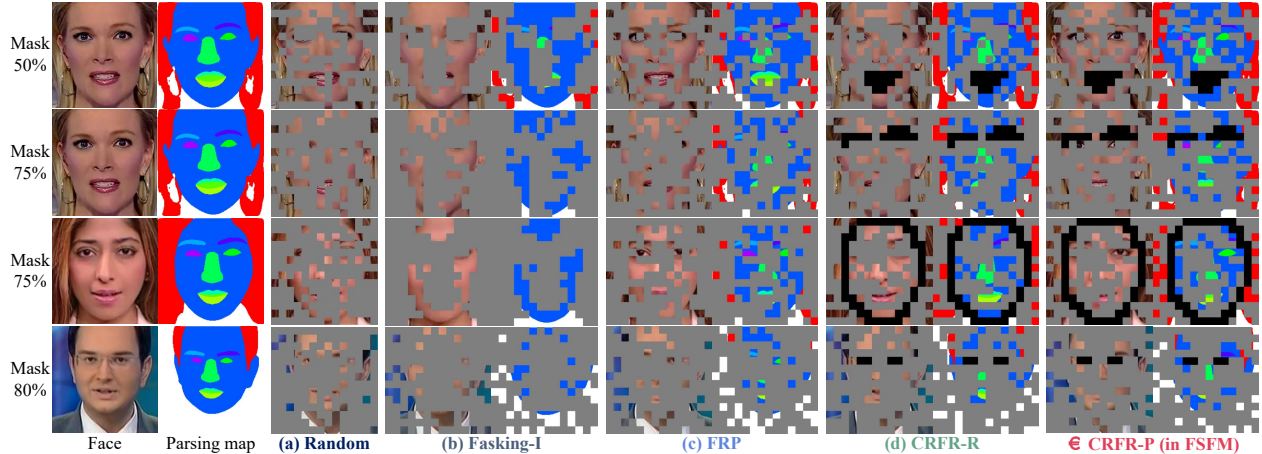


Figure 5. Additional visualizations of different facial masking strategies. (a) Random masking [45]. (b) Fasking-I adapted from [8]. (c) FRP: Facial Region Proportional masking (d) CRFR-R: Covering a Random Facial Region followed by Random masking. (e) CRFR-P: Covering a Random Facial Region followed by Proportional masking.

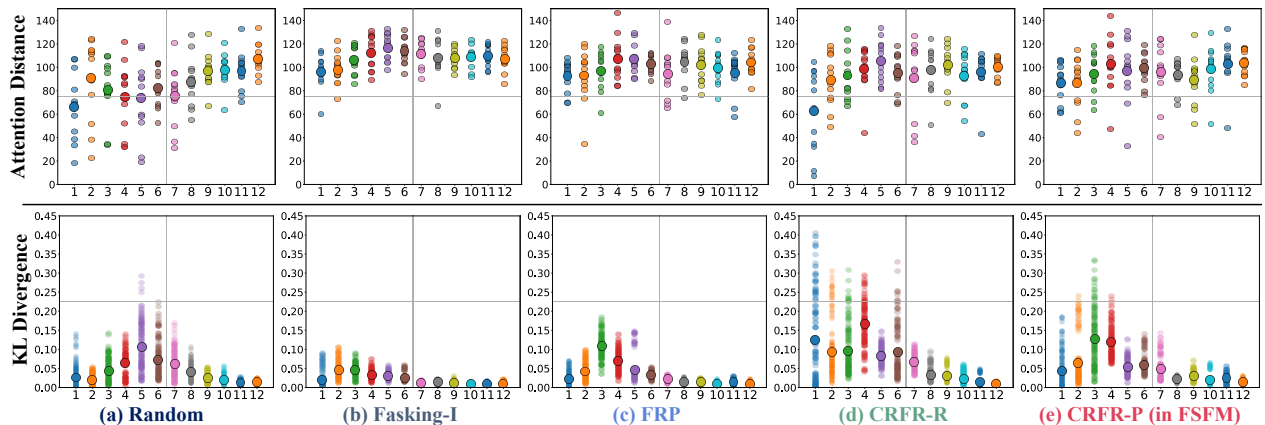


Figure 6. The mean attention distance (*Top*) and Kullback-Leibler divergence (*Bottom*) of each attention head (small dot) across all blocks (x -axis) in the ViT-B/16 encoder pretrained by MAE [45] with (a) random masking, (b) Fasking-I, (c) FRP, (d) CRFR-R, and (e) CRFR-P masking strategies, along with the average one (large dot) for each block.

gence in CRFR-R versus the simple random masking counterparts and CRFR-P versus the FRP counterparts. This suggests that the model is compelled to look at different regions after fully masking a facial region.

Overall, the model pretrained with FRP lacks diversity across attention heads, while CRFR-R shows excessive diversity. Similar to the phenomenon observed in mean attention distance, CRFR-P strikes a balance in KL divergence across different heads, which also seems to act as a co-effect of FRP and CRFR-R counterparts, implicating appropriate attention to different key tokens.

B.3. Key regions?

To uncover which regions of real faces are critical to the pretrained model, we visualize the mean attention map of the last block and overlay it onto the input face in Fig. 7, as the pretext decoder or downstream head follows the last

block. We can observe significant attention differences in the salient regions across different masking strategies. At first glance, the attention regions from simple random masking appear to cover the entire face. However, it predominantly highlights the skin, which can be easily recovered from visible neighboring patches, ignoring more challenging key regions. This suggests that the model solves face reconstruction through shortcuts instead of learning meaningful features. Similarly, the attention in Fasking-I is distributed across skin and background regions, as expected. While FRP and CRFR-R activate more attention areas, they still struggle to focus on key facial regions. In contrast, CRFR-P highlights attention across key regions like the eyes, eyebrows, and nose, indicating that the pretrained model tackles the challenge head-on: focusing on meaningful region-level features beyond just low-level pixels of real faces.

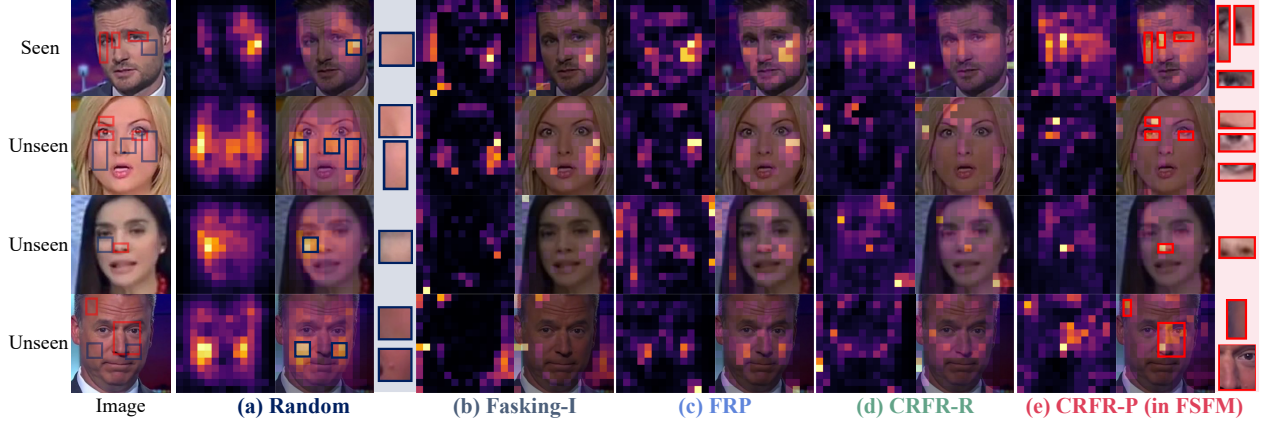


Figure 7. Visualization of the self-attention map averaged across all heads from the last block of the ViT-B/16 encoder pretrained by MAE [45] with (a) random masking, (b) Fasking-I, (c) FRP, (d) CRFR-R, and (e) CRFR-P masking strategies. The rectangles in (a) and (e) highlight the regions of interest (ROI) for comparison. All faces, except for the first row, are from the test set and were unseen during pretraining.

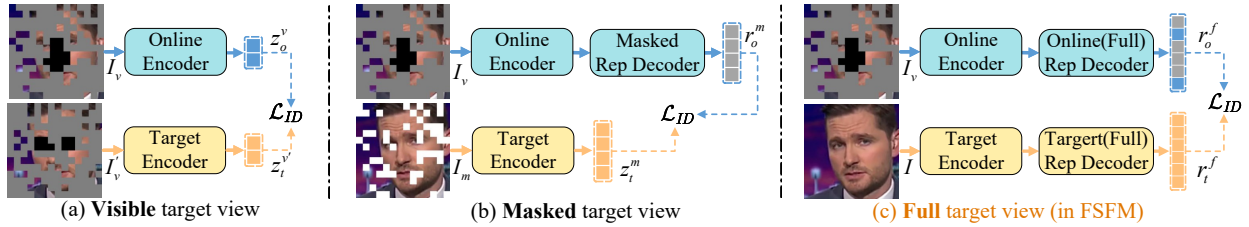


Figure 8. Comparison of typical target views and designs adapted for FSFM, derived from self-supervised pretraining methods that integrate both MIM and ID (or Siamese encoder architecture). (a) Visible patches from a different mask [4, 64, 103, 128]. (b) Masked patches from the same mask [17]. (c) Full patches without masking [1, 55, 96, 119, 131].

In summary, the CRFR-P masking strategy effectively directs attention to critical facial regions with appropriate range and diversity for both intra-region consistency and inter-region coherency, enabling the pretrained facial model to avoid trivial solutions (shortcuts) and capture the intrinsic properties of real faces. Furthermore, we hope this section provides new insights into fundamental face representation.

C. Connection and analysis of ID in FSFM

We illustrate the relation and distinction between our method and previous works that integrate ID (or Siamese encoder architecture) into MIM (or degraded input). While these hybrid approaches have demonstrated effectiveness in natural vision and face analysis, our empirical studies reveal that face security tasks necessitate more precise and reliable semantic alignment from the ID network. In response, we distinguish key designs such as target view&network structure, data augmentation, and loss function, which support local-to-global correspondences in FSFM.

C.1. Target view and network design

From the perspective of the input view, the online/student branch typically processes visible patches from the masked

image, while the target/teacher branch varies across methods. Thus, we incorporate different target views and design paradigms into FSFM, as shown in Fig. 8. (a) Visible patches from a different mask [4, 64, 103, 128]: the online and target encoders produce latent features z_o^v and z_t^v for subsequent contrast learning. (b) Masked patches from the same mask [17]: to align the representation r_o^m of masked patches with the encoded target z_t^m , a masked representation (rep) decoder predicts r_o^m from the visible tokens z_o^v output by the online encoder. This decoder computes cross-attention between masked tokens (as Q) and full tokens (as K and V), following the latent regressor in CAE [17] and resembling the prompting decoder in [49]. (c) Full patches without masking [1, 55, 96, 119, 131]: some methods [1, 119, 131] are decoder-free designs that match visible online features z_o^v with full target features z_t^f to compute $\mathcal{L}_{ID}(z_o^v, z_t^f)$. Unlike CMAE [55], which introduces a feature/rep decoder after the online encoder, *i.e.*, $\mathcal{L}_{ID}(r_o^f, z_t^f)$, we add an additional target rep decoder to compute $\mathcal{L}_{ID}(r_o^f, r_t^f)$ in a disentangled representation space. *i.e.*, Siamese rep decoders. This design further reduces the gap in distribution between low-level pixel features and high-level semantic representations.

Method	Pretrain or Init	DG FAS Technique					OCI→M		OMI→C		OCM→I		ICM→O		Avg.	
		DM	AL	CL	ML	PL	HTER↓	AUC↑	HTER↓	AUC↑	HTER↓	AUC↑	HTER↓	AUC↑	HTER↓	AUC↑
Base model																
ViT-B [28]*	Scratch						15.25	90.07	36.98	63.94	10.75	96.09	37.50	66.03	25.12	79.03
ViT-B [28]*	Sup.(IN)						5.00	97.29	11.51	95.61	10.60	94.03	17.35	88.35	11.12	93.82
MAE [45] ViT-B*	SSL.(LN)						8.17	97.37	27.91	77.90	18.02	91.54	25.36	80.76	19.86	86.89
DINO [11] ViT-B*	SSL.(LN)						7.92	97.09	21.28	87.79	21.35	84.48	17.44	89.75	17.00	89.78
MCF [103] ViT-B*	SSL.(LFC)						6.33	98.29	21.40	86.72	13.13	95.15	16.76	89.59	14.41	92.44
FSFM ViT-B (Ours)*	SSL.(VF2)						6.58	97.43	4.30	99.10	14.63	90.96	<u>10.02</u>	96.23	<u>8.88</u>	<u>95.93</u>
ViT-based specialized method (Venue)																
ViTranZFAS [33] (IJCB'21)*	Init.(IN)						10.95	95.05	14.33	92.10	16.64	85.07	15.67	89.59	14.40	90.45
TransFAS [105] (TBiom'22)*	Init.(IN)	✓					7.08	96.69	9.81	96.13	10.12	95.53	15.52	91.10	10.63	94.86
TTN-S [106] (TIFS'22)*	Init.(IN)	✓					9.58	95.79	9.81	95.07	14.15	94.06	12.64	94.20	11.55	94.78
DiVT-V [67] (WACV'23)*	Init.(IN)			✓	✓		10.00	96.64	14.67	93.08	5.71	<u>97.73</u>	18.06	90.21	12.11	94.42
TTDG-V [134] (CVPR'24)*	Init.(IN)		✓				4.16	98.48	7.59	98.18	<u>9.62</u>	98.18	10.00	96.15	7.84	97.75

Abbreviation: Sup-Supervised SSL-Self-Supervised Init-weight initialization IN-ImageNet DG-Domain Generalization

DG FAS Technique: DM-Depth Maps AL-Adversarial Learning CL-Contrastive Learning (or triplet, similarity loss) ML-Meta Learning PL-Prototype Learning

Table 5. Cross-domain evaluation on face anti-spoofing (FAS), *using visual-only ViT-based models without including the supplementary data in [54]. For a fair comparison, the results of specialized methods are cited from the original papers. **Best results**, second-best.

Method	Pretrain or Init	Train Set	Test Set Video-level AUC(%)↑				Avg. ΔOurs	Method	Pretrain or Init	Train Set	Test Set Frame-level AUC(%)↑				Avg. ΔOurs
			CDFV2	DFDC	DFDCP	WDF					CDFV2	DFDC	DFDCP	WDF	
Base model															
Xception [22]	Sup(IN)	FF++	76.39	70.62	72.24	76.11	14.0↑	Xception [22]	Sup(IN)	FF++	69.52	68.20	68.94	68.83	15.1↑
EfficientNet-B4 [95]	Sup(IN)	FF++	79.81	71.85	66.95	76.42	14.1↑	EfficientNet-B4 [95]	Sup(IN)	FF++	73.37	69.47	64.37	71.95	14.2↑
ViT-B [28]	Scratch	FF++	64.08	66.73	72.62	60.36	21.9↑	ViT-B [28]	Scratch	FF++	61.14	64.27	69.00	60.68	20.2↑
ViT-B [28]	Sup(IN)	FF++	<u>86.24</u>	74.48	82.11	81.20	6.9↑	ViT-B [28]	Sup(IN)	FF++	<u>77.43</u>	71.09	74.07	<u>75.86</u>	9.4↑
MAE [45] ViT-B	SSL(IN)	FF++	79.51	75.93	87.10	80.96	7.0↑	MAE [45] ViT-B	SSL(IN)	FF++	72.64	72.18	<u>79.81</u>	73.94	9.4↑
DINO [11] ViT-B	SSL(IN)	FF++	80.47	76.90	84.64	82.06	6.9↑	DINO [11] ViT-B	SSL(IN)	FF++	73.88	<u>72.78</u>	<u>77.31</u>	75.08	9.2↑
MCF [103] ViT-B	SSL(LFC)	FF++	80.25	73.61	82.55	79.79	8.8↑	MCF [103] ViT-B	SSL(LFC)	FF++	73.16	<u>69.63</u>	75.78	74.10	10.8↑
CLIP [83] ViT-B	VLP(WIT)	FF++	78.95	73.83	82.38	78.60	9.5↑	CLIP [83] ViT-B	VLP(WIT)	FF++	73.02	70.66	77.46	72.04	10.7↑
FSFM ViT-B (Ours)	SSL(VF2)	FF++	91.44	83.47	89.71	86.96	-	FSFM ViT-B (Ours)	SSL(VF2)	FF++	85.05	80.20	85.50	85.26	-

Abbreviation: Sup-Supervised SSL-Self-Supervised VLP-Vision Language pretraining Init-weight initialization

Dataset: IN/IM natural images [25] LFC/20M facial images [103] WIT/400M (natural image, text) pairs [83] VF2/3M facial images [10]

Table 6. Cross-dataset evaluation on deepfake detection (DfD), adding CLIP [83] ViT-B/16 image encoder as a base model. Left: video-level AUC, Right: frame-level AUC. All base models are trained on FF++ (c23) and tested on unseen datasets. Avg.ΔOurs denotes the average AUC difference between our FSFM and other methods. **Best results**, second-best.

Based on our ablations (in the main paper) of downstream face security tasks, FSFM performs better when using full patches as the target view alongside Siamese rep decoders. By predicting the entire face representation from visible parts, the ID network aligns global and local views of the same face. In light of this, FSFM structures the encoded space with semantically complete facial representations through "local-to-global" correspondences [11], which endows the encoder with strong facial discriminability.

C.2. Data augmentation

Most ID methods [11, 14–16, 36, 44] rely on strong data augmentations, including spatial and color transforms, to prevent trivial solutions. For MIM, applying strong augmentations, such as color enhancements, is suboptimal [45], as masking corruption itself effectively regularizes the pretext task. This is further evident in methods [55, 64, 119] that combine MIM and ID, where only simple augmentations—random size cropping or flipping—are applied to the masked input of the online branch, while strong or simple augmentations are used for the full (unmasked) target view.

In contrast, our FSFM behaves well without any data augmentation in either the online or target branches. This may stem from the semantic integrity preserved in unaugmented inputs, which benefits the learning of global face

identity [103], especially in face security tasks where forgery and spoofing cues may be implicit anywhere. Additionally, the proposed CRFR-P masking strategy inherently introduces spatial variance tailored to facial structures, rendering simple augmentations (crop and flip) unnecessary. Consequently, FSFM processes only a single view per face image.

C.3. Loss function for ID

We consider two main types of loss functions for ID: contrastive [14, 16] and non-contrastive [15, 36]. Contrastive loss pulls positive views from the same sample together and pushes negative views from different samples apart. We use the widely adopted InfoNCE [80] as the contrastive loss. Non-contrastive loss maximizes the similarity of positive representations only. We use mean squared error (MSE) in BYOL [36] and negative cosine similarity (NCS) in SimSiam [15] as non-contrastive loss, respectively, but in an asymmetric formulation, as detailed in the main paper.

In FSFM, we observe that NCS outperforms the contrastive loss InfoNCE, even though methods combining MIM and ID [55, 64, 103, 119] favor the latter. We speculate this is because, in large-scale pretraining on real faces, the inter-image contrast introduced by negative sample pairs—pushing one real face away from others—does not help our model learn representations that are beneficial

Method	Pretrain or Init	OCI→M		OMI→C		OCM→I		ICM→O		Avg.	
		HTER↓	AUC↑	HTER↓	AUC↑	HTER↓	AUC↑	HTER↓	AUC↑	HTER↓	AUC↑
Base model											
ViT-B [28]	Scratch	15.37	90.73	35.37	68.23	14.75	94.18	31.65	71.55	24.28	81.17
ViT-B [28, 54]	Sup(IN)	3.52	98.74	2.42	99.52	8.45	96.91	11.86	94.62	6.56	97.44
MAE [45] ViT-B	SSL(LN)	10.32	94.87	15.91	89.96	15.54	91.13	16.51	90.29	14.57	91.56
DINO [11] ViT-B	SSL(LN)	6.73	97.15	13.44	93.90	14.27	93.56	15.55	90.99	12.50	93.90
MCF [103] ViT-B	SSL(LFc)	4.00	98.84	8.46	96.90	8.02	97.39	10.70	95.64	7.80	97.19
CLIP [83] ViT-B	VLP(WIT)	4.29	98.76	5.00	98.89	7.14	97.92	6.09	98.12	5.63	98.42
FSFM ViT-B (Ours)	SSL(VF2)	3.78	99.15	3.16	99.41	4.63	99.03	7.68	97.11	4.81	98.68

Abbreviation: Sup-Supervised SSL-Self-Supervised VLP-Vision Language pretraining Init-weight initialization

Dataset: IN-ImageNet1K [25] LFc-LAION FACE cropped [103] WIT-WebImageText [83] VF2-VGGFace2 [10]

Table 7. Cross-domain evaluation on face anti-spoofing (FAS), adding CLIP [83] ViT-B/16 image encoder as a base model. **Best results, second-best.**

for face security tasks. Thus, we adopt asymmetric NCS by default to learn intra-face correspondences by matching the online anchor view with the target view of the same sample.

D. More implementation details

D.1. pretraining settings

We set the mask ratio r to 0.75, similar to the baseline [45], as our ablation shows that this high ratio is also favorable for our FSFM. We do not use any data augmentation (not even crop and flip used in [45]) and only normalize the input faces during pretraining. We empirically set the loss weights λ_{fr} and λ_{cl} to 0.007 and 0.1, respectively. The projection and prediction heads are 2-layer MLPs following BYOL [36], with batch normalization (BN) replaced by layer normalization (LN) for our ViT-based architecture. The EMA momentum coefficient for updating the target branch starts from 0.996 and increases with a cosine scheduler, following BYOL [36]. We pretrain our model from scratch for 400 epochs on 4 NVIDIA RTX A6000 GPUs. Other settings follow the defaults in MAE [45]: we use the AdamW [75] optimizer with momentum $\beta_1 = 0.9$, $\beta_2 = 0.95$; we apply the linear lr scaling rule [35] with a base learning rate of $1.5e-4$; we adopt a cosine decay [76] learning rate schedule with a warmup epoch of 40; we maintain the effective batch size as $4096 = 256$ (batch size per GPU) $\times 4$ (GPUs) $\times 4$ (accumulated gradient iterations).

D.2. Finetuning settings in downstream tasks

For finetuning the ViTs from FSFM and other pretrained models, we adopt identical settings except for weight initialization, detailed below.

Deepfake Detection We use the c23 (HQ) version of FF++ [84] with official train/val splits for finetuning. We sample 128 frames per real video (the original YouTube subset) and 32 frames per forgery video (including Deepfakes, Face2Face, FaceSwap, and NeuralTextures subsets). We follow the official test split in other unseen datasets for testing, including CDFV2 [65], DFDC [27], DFDCp [26], and WDF [137]. We sample 32 frames per testing video. We use DLIB [59] to extract faces (without alignment and parsing) and resize them to 224×224 . As WDF already pro-

vides 224×224 facial images, we directly use its test set. We add only one linear layer as the binary classifier after averaging all non-CLS token features. We set the batch size to 64, the base learning rate to $2.5e-4$, and the finetuning epochs to 10 (50 for ViT-B Scratch). Other settings adhere to the MAE ImageNet finetuning recipe [45].

Face Anti-Spoofing In the main paper, we adopt the 0-shot MCIO setting (Protocol 1) in [54] and include CelebA-Spoof [124] as supplementary data for FAS finetuning. We set the batch size to 12 for each training domain. We append the MLP head after averaging all non-CLS token features instead of using CLS ones [54], to align with other face security tasks. Additionally, for a fair comparison with other visual-only ViT-based methods, we additionally follow [134] and report the best performance without including the supplementary data, as presented in Sec. E.1.

Diffusion Face Forgery Detection For the training set, we sample 32 frames from each real video (the original YouTube subset) and each forgery video (the Deepfakes subset) from FF++ (c23) [84]. For validation and testing sets, we follow the splits provided by the DiFF benchmark [18]. We use DLIB [59] to extract faces (without alignment and parsing) and resize them to 224×224 . We add one linear layer as the binary classifier after averaging all non-CLS token features. We set the batch size to 256, the base learning rate to $5e-4$, and the finetuning epochs to 50. Other settings adhere to the MAE ImageNet finetuning recipe [45].

E. Additional experimental results

E.1. Comparison with ViT-based FAS

In a fair comparison with visual-only ViT-based FAS methods, our method also significantly outperforms all base models, as shown in Tab. 5. FSFM surpasses most counterparts and ranks second in average metrics. TTDG-V [134], which introduces test-time domain generalization and explicit optimization goals for FAS, performs better than ours in two out of four target domains (M and I). While optimizing for a specific downstream task is beyond the scope of this study, incorporating special auxiliary supervision or domain generalization (DG) techniques into our pretrained

Method	Pretrain or Init	Test Subset (AUC% \uparrow)					Avg. w/o FF++
		FF++	T2I	I2I	FS	FE	
ViT-B [28]	Scratch	92.02	62.19	69.99	60.87	67.30	65.09
ViT-B [28]	Sup(IN)	99.15	33.38	35.83	52.20	55.42	44.21
MAE [45] ViT-B	SSL(IN)	99.25	33.01	32.88	47.77	58.70	43.09
DINO [11] ViT-B	SSL(IN)	99.30	33.85	36.02	60.37	63.18	48.35
MCF [103] ViT-B	SSL(LFc)	99.39	39.09	38.67	34.35	56.02	42.03
CLIP [83] ViT-B	VLP(WIT)	99.33	69.63	66.25	65.23	57.07	64.54
FSFM ViT-B	SSL(FF++ _o)	99.31	61.74	71.91	71.31	78.98	70.99

Table 8. Cross-dataset evaluation on DiFF benchmark [19], adding CLIP [83] ViT-B/16 image encoder as a base model. All base models are trained only on the FF++_DeepFake (c23) [84]. **Best results, second-best.**

model may further improve its generalization ability for face presentation attack detection.

E.2. Comparison with CLIP

Another line of representation learning, vision-language pretraining (VLP), particularly contrastive language-image pretraining (CLIP) [83], has shown remarkable zero-shot and generalization capabilities across diverse downstream tasks. Recent studies have successfully tailored CLIP to specific face security tasks, including deepfake detection [58, 90, 94], face anti-spoofing [39, 52, 69, 71, 91], and diffusion forgery detection [23, 68, 125]. These text-aided methods differ fundamentally from our FSFM, which is vision-only, self-supervised, and task-agnostic. Moreover, VLP demands extensive (image, text) data pairs along with significant computing resources for the additional text encoder. Despite these, we include CLIP as a base vision-language model (VLM) for comparison.

Specifically, we borrow the CLIP image encoder, also a ViT-B/16 but pretrained on 400M (image, text) pairs, and finetune it on downstream face security tasks under the same settings as other base models. We supplement its results on deepfake detection, face anti-spoofing, and diffusion face forgery detection in Tab. 6, Tab. 7, and Tab. 8, respectively. We can observe that CLIP ViT-B transfers better than other base vision models on FAS and DiFF tasks, benefiting from the extensive scale of multi-modal supervision. However, directly applying CLIP ViT-B to DfD exhibits inferior generalization. In contrast, our proposed FSFM also consistently outperforms CLIP ViT-B across downstream face security tasks.

F. More ablations and visualizations

F.1. Ablation studies

This subsection presents additional ablations. Unless otherwise stated, the default settings follow the main paper.

Effect of Masking Ratio r We also examine the impact of different masking ratios for CRFR-P masking on our pre-training framework. As shown in Tab. 9, FSFM achieves the best overall performance with a 0.75 masking ratio. Adopting lower masking ratios leads to trivial reconstruction and

Component	Setting	Deepfake Detection		Face Anti-spoofing	
		F-AUC \uparrow	V-AUC \uparrow	HTER \downarrow	AUC \uparrow
Masking ratio r	0.35	73.92	79.56	15.84	90.02
	0.50	74.31	79.48	21.57	84.09
	0.65	74.92	80.13	17.76	87.37
	0.75	76.39	82.31	17.44	88.26
	0.85	75.40	80.83	19.19	86.13
pretraining model		Size			
Model size (parameters)	ViT-S/16(22M)	74.80	80.20	19.32	89.13
	ViT-B/16(86M)	76.39	82.31	17.44	88.26
	ViT-L/16(303M)	77.43	83.15	16.23	93.13

Table 9. Ablations on deepfake detection (DfD) and face anti-spoofing (FAS) with average metrics. The model is pretrained on FF++_o [84]. Default settings are shaded in gray.

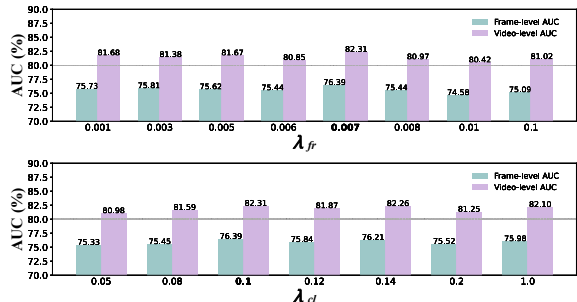


Figure 9. Ablations of loss weights on deepfake detection (DfD) with average metrics. The model is pretrained on FF++_o [84]. Default: $\lambda_{fr} = 0.007$, $\lambda_{cl} = 0.1$.

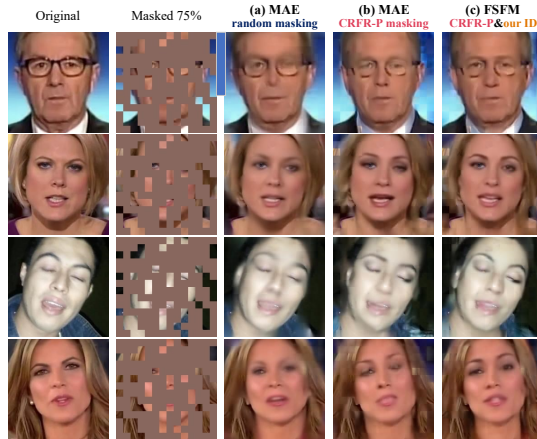


Figure 10. **Reconstruction Visualization** of real face images with a masking ratio of 75%, using MIM models pretrained from: (a) a naive MAE with simple random masking [45], (b) a naive MAE with our CRFR-P masking, and (c) our FSFM. All models were pretrained on the train and validation sets of FF++_o [84] without adversarial learning, for 400 epochs. Images are from the test set.

alignment tasks due to more available information. Conversely, using a higher masking ratio makes pretext tasks too challenging to learn sufficient facial representations for downstream face security tasks. Accordingly, we select a 75% masking ratio as the default setting.

Effect of Model Scaling Tab. 9 also shows that FSFM benefits from larger model sizes when pretrained on FF++_o.

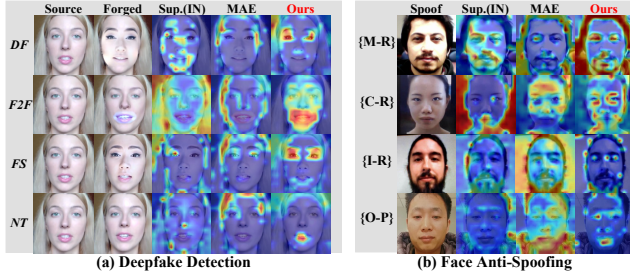


Figure 11. **CAM Visualization.** (a) DfD on various manipulations from FF++ [84]. (b) FAS on the MCIO protocol. FSFM highlights forgery artifacts and spoof clues. Images are from the test set.

The transfer performance on downstream face security tasks improves as the model scales up. Due to limited computing resources, we were unable to pretrain larger models on more face images, but we aspire to explore this in future work.

Effect of Loss Weight To explore the impact of the reconstruction and distillation losses, we vary various loss weights, *i.e.* λ_{fr} and λ_{cl} . Results in Fig. 9 show that the configuration ($\lambda_{fr} = 0.007$, $\lambda_{cl} = 0.1$) performs better on challenging cross-dataset deepfake detection.

F.2. Visualizations

Reconstruction To demonstrate the superiority of the facial representations pretrained with FSFM, we further follow MAE [45] to visualize reconstruction results, as shown in Fig. 10. We can see that FSFM demonstrates better reconstruction quality concerning intra-region consistency (preserving fine-grained textures within facial regions), inter-region coherency (maintaining spatial relationships across regions), and local-to-global correspondence (aligning local appearance with global facial looking).

CAM We provide additional CAM visualizations in Fig. 11, which are consistent with the observations in the main paper, further substantiating the effectiveness of our method.